Revision 2 December 7, 2014

NMR and Computational Molecular Modeling Studies of Mineral Surfaces and Interlayer Galleries: A Review

R. James Kirkpatrick,[1] Andrey G. Kalinichev,[2] Geoffrey M. Bowers,[3] A. Ozgur Yazaydin,[4,5] Marimuthu Krishnan,[4,6] Moumita Saharay,[4,7] Christin P. Morrow[4,8]

[1] College of Natural Science, Michigan State University, East Lansing, Michigan 48824, United States. rjkirk@msu.edu.

[2]Laboratoire SUBATECH, Ecole des Mines de Nantes, Nantes Cedex 3, France, 44307. kalinich@subatech.in2p3.fr.

[3]Division of Chemistry and Department of Materials Engineering, Alfred University, Alfred, New York, 14802, United States. bowers@alfred.edu.

[4]Department of Chemistry, Michigan State University, East Lansing, Michigan 48824, United States. yazaydin@msu.edu.

[5]Department of Chemical Engineering, University College London, London, WC1E 7JE, United Kingdom.

[6]Center for Computational Natural Sciences and Bioinformatics, International Institute of Information Technology, Gachibowli, Hyderabad, India, 500 032. m.krishnan@chemistry.msu.edu.

[7] Department of Physics, Osmania University, Hyderabad, Telengana, India. saharaym@chemistry.msu.edu.

8. Current address: Alcon Laboratories, 6201 South Freeway, Fort Worth, TX 76134.

christinpmorrow@gmail.com.

Abstract

This paper reviews experimental nuclear magnetic resonance (NMR) and computational molecular dynamics (MD) investigations of the structural and dynamical behavior of cations, anions, H_2O and CO_2 on the surfaces and in the interlayer galleries of layer-structure minerals and their composites with polymers and natural organic matter (NOM). The interaction among mineral surfaces, charge balancing cations or anions, H_2O, CO_2, and NOM are dominated by Coulombic, H-bond, and van der Waals interactions leading to statically and dynamically disordered systems and molecular scale processes with characteristic room-temperature frequencies varying from at least as small as 10^2 Hz to greater than 10^{12} Hz. NMR spectroscopy provides local structural information about such systems through the chemical shift and quadrupolar interactions and dynamical information at frequencies from the sub-kHz to GHz ranges through the T_1 and T_2 relaxation rates and line shape analysis. It is often difficult to associate a specific structure or dynamical process to a given NMR observation, however, and computational molecular modeling is often effective in providing a much more detailed picture in this regard. The examples discussed here illustrate these capabilities of combining experimental NMR and computational modeling in mineralogically and geochemically important systems, including clay minerals and layered double hydroxides.

Keywords: Mineral surfaces, mineral-fluid interactions, clay minerals, natural organic matter, NMR, molecular dynamics, computational modeling, layered double hydroxides.

Introduction

Layer-structure phases such as clays and layered double hydroxides (LDHs) are important natural minerals and industrial materials with high surface areas and often large ion exchange capacities (Brindley and Brown, 1980; Bailey 1988). The interaction of aqueous fluids with these phases is important in many geochemical and industrial situations and can occur both on external surfaces and within the two dimensional, nanometer-scale confined spaces of the interlayer galleries (e.g., Sposito, 1984; Skipper et al., 2006). Investigating the structures of the interlayers and near-surface regions of these phases is very challenging, because the individual (alumino)silicate layers of clays and the hydroxide layers of LDHs often show significant stacking disorder and because the interlayers and near-surface fluid environments are typically dynamically and statically disordered (Brindley and Brown, 1980; Newman et al., 1998; Marcelin et al., 1989; Kirkpatrick, et al., 2005b; Marry et al., 2008, 2011; Morrow et al., 2013; Ngouana and Kalinichev, 2014). Similarly, organic compounds and condensed organic matter are equally important in low temperature geological environments (e.g., Sposito, 1984; Stevenson, 1994; Tipping, 2002; Wershaw, 2004; Leenheer, 2009). Most naturally occurring organic matter (NOM), such as the humic substances in soils and natural waters, is highly disordered, and its interactions with mineral surfaces (often clays), water, dissolved species, and CO_2 and other fluids is equally difficult to investigate (e.g., Murphy and Zachara, 1995; Schulten and Schnitzer, 1997; Shevchenko and Bailey, 1998; Piccolo, 2001, 2002; Ritchie and Perdue, 2003; Sutton and Sposito, 2005; Iskrenova-Tchoukova et al., 2010; Kalinichev, 2013). Characterization of the interlayer and surface regions of clay minerals, LDHs and NOM and the fluid near NOM molecules requires understanding of the distribution of local (nearest neighbor [NN] and next nearest neighbor [NNN]) atomic arrangements; the average structure (e.g.,

average coordination and bond distances and angles); the diffusional, site exchange, vibrational, rotational, and translational dynamics; and the energetics of the interactions. The important molecular processes that control these interactions have characteristic frequencies that vary over many orders of magnitude at ambient temperatures, from at least as small as 10^2 Hz - 10^4 Hz to > 10^{12} Hz (e.g., Cygan, 2001; Wang, et al., 2005, 2006; Bowers et al., 2011)

The importance of dynamical behavior in these systems is the result of the dominance of electrostatic (Coulombic and hydrogen-bond [H-bond]) and dispersive (van der Waals) interactions, rather than the stronger covalent bonding that dominates the aluminosilicate structure of many minerals (Cygan and Kubicki, 2001; Cygan, 2001; Gale, 2001; Kalinichev, 2001; Wang et al., 2001; Cygan et al., 2004, 2009). H-bonding is very significant for hydrous systems, and H-bond strengths typically range from 10 to 25 kJ/mol. The thermal energy at room temperature is ~2.5 kJ/mol, sufficient to occasionally overcome activation barriers of this magnitude (e.g., Morrow, et al., 2013). The interactions between CO_2 molecules are even weaker, with the dimer binding energy being approximately 2 to 3 kJ/mol (Saharay and Balasubramanian, 2007).

The combination of nuclear magnetic resonance spectroscopy (NMR) and computational, molecular-scale modeling has been particularly effective in assessing the structures and dynamics of disordered geological materials across this range of temporal and spatial scales (Kalinichev et al., 2000; Kirkpatrick et al., 2005c; Bowers et al., 2011; Morrow et al., 2013). This paper reviews results that illustrate how the combination of these two methods provides otherwise unobtainable structural and dynamical information about interlayer galleries and near-surface fluid regions.

NMR spectroscopy is the only currently available element-specific experimental method that simultaneously probes local structure and dynamics on the Å to nm length scale and the sub-kHz to GHz frequency ranges in disordered systems such as clays, LDHs, and NOM. NMR probes local structure through the chemical shift and nuclear quadrupolar interactions, longer-range structural relationships through dipolar and scalar couplings between nuclei, and dynamics through T_1 and T_2 relaxation rates and line shape analysis (see, e.g., Slichter, 1990). T_1 (longitudinal) relaxation is sensitive to processes near the Larmor frequency (the resonance frequency of the observed nucleus at the applied magnetic field). For modern spectrometers these frequencies are typically in the 10 MHz to 1 GHz range, depending on the instrument and observed nucleus. T_2 (transverse) relaxation and line shape analysis are sensitive to lower frequencies, typically in the 1 – 100 kHz range. Both of these frequency ranges are much lower than those probed by vibrational spectroscopy but are often relevant to processes in interlayers and at fluid-mineral interfaces (e.g., Wang, et al., 2005, 2006; Bowers et al., 20089a, 2011, 2014b). Unlike quasieleastic neutron scattering, that can simultaneously probe the structure and dynamics in these frequency ranges for hydrous systems through observation of hydrogen isotopes (e.g., Michot et al., 2012), NMR can observe many, although not all, elements, including ^{1}H, ^{2}H, many alkali and alkaline earth elements, many groups III – VIII elements, and some transition metals. However, it is often difficult to associate an observed NMR signal with a unique molecular scale structure or dynamical processes, especially for disordered systems (e.g., Hou et al., 2002). In many cases interpretation is based on data for well understood reference compounds and on the variation of the observed parameter with composition, temperature, and water content (relative humidity). Because the interaction among the (alumino)silicate or hydroxide layers and the interlayer/interfacial ions, H_2O and organic molecules is dominated by

electrostatic and dispersive forces, it is often necessary to investigate ^2H_2O, cation and anion line shapes over temperatures from -80 or -100^oC to near or above room temperature to obtain a clear picture of the dynamical behavior (Weiss, et al., 1990; Kim et al., 1996; Bowers et al., 2008a, 2011; 2014b).

Computational molecular modeling can often provide the missing molecular scale insight needed to interpret NMR results. Likewise, the modeling results can often motivate productive directions for exploration via experimental NMR. Molecular dynamics (MD) and related enhanced sampling methods such as metadynamics and potential of mean force (PMF) calculations have been especially effective in this regard (Kirkpatrick et al., 1999; Hou et al., 2002; Xu et al., 2006; Iskrenova-Tchoukova, et al., 2010; Morrow et al., 2013). This is because, like NMR, they can effectively investigate structure on molecular length scales and simultaneously provide information about dynamic behavior with correlation times up to ns or ms (Cygan and Kubicki, 2001; Cygan et al., 2004, 2009; Kumar et al., 2006; Ferrage et al., 2011; Kalinichev, 2013). In addition, molecular simulations can provide important energetic constraints that can, for instance, help rationalize layer spacings and swelling behavior for clays and LDHs obtained from powder X-ray diffraction (Boek et al., 1995; Smith et al., 1998; Wang et al., 2001; Cygan et al., 2004; Morrow, 2013). Monte Carlo (MC) methods can provide structural and energetic information similar to MD, but not dynamical information. All the results described here use MD or related enhanced sampling methods.

MD simulations of the type discussed here model the atomic scale evolution of an equilibrium system of atoms or small molecules through time (Allen and Tildesley, 1987; Cygan and Kubicki, 2001; Gale, 2001; Cygan et al., 2004). They, thus, provide information about changes in local and average structure; dynamical information such as diffusion coefficients,

surface residence times, H_2O residence times in cation hydration shells, vibrational, rotational, translational, and site hopping frequencies; and the system energy. Classical MD uses sets of interatomic potentials (force field parameters) to describe the atomic interactions. No matter how these potentials are determined, all inevitably have an empirical component and must be tested against experimentally observed structural, dynamical, and thermodynamic properties. There have been extensive efforts to develop effective force fields for geochemically relevant systems, and currently available sets for mineral systems have been well tested (Cygan, et al., 2004; Heinz, et al., 2012; see Gale, 2001 for a review). Most of the simulations described here use the CLAYFF force field (Cygan et al., 2004) to describe the inorganic species. This force field has been shown to be very effective for many oxide materials and has been applied to many simulations related to the structure of (alumino)silicate minerals; the structure of fluid-mineral interfaces; surface sorption; the structure, dynamics and energetics of clay interlayers and zeolite pores; and the interaction of organics species with oxide minerals. Cygan et al. (2009) give a review of the applications up to that date, and Ebrahimi, et al. (2014), Ngouana, et al., (2014), Teich-McGoldrick, et al., (2014), and Wang, et al. (2014) are examples of more recent applications.

Using modern supercomputers, MD can readily model geochemically relevant systems containing up to millions of atoms for times up to ms, although ~10^{-8} s is more common. Thus, these methods can provide dynamical information at frequencies of the order of and greater than the GHz range. Traditional quantum chemical calculations or ab initio MD (AIMD) methods often connect less well with NMR results for clay minerals, LDHs, and NOM of the type we address here, because they either cannot easily model large enough systems to realistically investigate their compositional and structural disorder or do not readily provide sufficient

dynamical information on time scales longer than ~10^{-11} s. To effectively use MD methods to study solid-fluid interactions, it is necessary to have a good structural model for the material. For mineral surfaces, this is typically a crystal structure obtained from diffraction methods, although it is often necessary to make assumptions about the specific local state of order, such as the Al,Si distribution in the tetrahedral sites of phyllosilicate minerals and the Mg,Al distribution in the octahedral sites of clays and LDHs (e.g., Cadars et al., 2011; 2012). NOM is structurally and compositionally very diverse. Structures for it for used in molecular simulations are less well developed than for layer structure minerals, but there are several models in use (e.g, Davies et al., 1997; Schulten and Schnitzer, 1997; Sein et al., 1999; Sutton et al., 2005; Kalinichev and Kirkpatrick, 2007; Iskrenova-Tchoukova et al., 2010). There is a need for additional work in this area (Sutton and Sposito, 2005; Schaumann and Thiele-Bruhn, 2011; Kalinichev, 2013). pH dependent negative charge development on NOM typically arises from protonation/deprotonation of carboxylic groups (pKa ~ 4) and phenolic and amine groups (pKa ~9). In most MD simulations, this protonation state is defined *a priori* and does not change during the simulation.

A Brief History

Nuclear magnetic resonance was discovered by Isidor Rabi in molecular beams in 1938 (Rabi et al., 1938) and later expanded to solids and liquids by Felix Bloch (Bloch et al., 1946) and Edward Purcell (Purcell et al., 1946). Rabi, Bloch and Purcell all received Nobel prizes for their work. Development of NMR theory, instrumentation and applications proceeded rapidly through the 1950s, and the first commercial NMR spectrometers became available in the early 1960s. Application to clay minerals dates at least to the late 1960's, with the early work focusing on adsorbed and interlayer water (e.g., Hecht et al., 1966; Touillau et al., 1968; Woessner and

Snowden, 1969; Hougardy et al., 1977; Grandjean, 1977; Fripiat, 1984; and many others). With the advent of the pulse-Fourier transform methods of spectral acquisition, high field superconducting magnets, and the routine use of magic angle sample spinning (MAS) in the late 1970s and early 1980s, it became possible to obtain spectra for a wider variety of nuclei with much higher resolution and signal/noise ratios than with previous instrumentation. Applications to mineralogical and geochemical problems advanced rapidly, including investigations of the structure and dynamical behavior of minerals, glasses, melts, and natural organic matter. For clay minerals and LDHs it became possible to study the (alumino)silicate or hydroxide layers using ^{17}O, ^{27}Al, and ^{29}Si NMR (e.g., Lippmaa et al., 1980; Kinsey et al., 1985, Weiss, et al., 1987, and many others) Similarly, adsorbed and interlayer cations could be probed using for instance ^{6,7}Li, ^{23}Na, ^{39}K, ^{43}Ca, ^{113}Cd, and ^{133}Cs, and anions (including oxyanions) could be probed with ^{13}C, ^{31}P, ^{35}Cl, and ^{77}Se. Water molecules could be investigated using ^{1}H and ^{2}H, which had been used extensively earlier (e.g., Marcelin et al., 1989; Weiss et al., 1990; Kim et al, 1996; Sullivan et al., 2000; Hou et al., 2002; Bowers et al., 2008b). The structure of NOM has been investigated extensively by ^{13}C NMR (e.g., Wershaw et al., 1988; Boutton et al., 1994; Derenne and Tu, 2014, and many others). Its interaction with water, cations and anions can be investigated for the same set of nuclei as for clays and LDHs. There have been many published studies using these techniques in recent years and several other recent reviews on this subject (e.g., Schaumann, and Thiele-Bruhn, 2011; Kalinichev, 2013).

The fundamental theory behind computational molecular dynamics modeling was developed by Alder and Wainwright (1959) and Rahman (1964) and grew rapidly through the 1960s and 1970s. Widespread application to large chemical, geochemical and biological systems began with the routine availability of computers in the 1970s and 1980s (see, e.g., Allen and

Tildesley, 1987). Much of the history of its development, the details for the methods, and applications in the geosciences has been described in Reviews in Mineralogy and Geochemistry v. 42, Molecular Modeling Theory: Applications in the Geosciences (Cygan and Kubicki, 2001 and individual chapters therein) and will not be further reviewed here. Application of computational molecular modeling methods to mineral-water interfaces and clay minerals goes back to at least the mid-1980s (Mulla et al., 1984) and expanded rapidly beginning in the 1990s (e.g., Boek et al., 1995; Chang et al., 1997; Teppen et al., 1997; Smith, 1998, Greathouse et al., 2000; Wang et al., 2005, 2006; Skipper et al., 2006; Cygan et al., 2009; Kalinichev, 2014). Application to LDHs and similar compounds began somewhat later but are now widespread (e.g., Aicken et al., 1997; Newman et al., 1998; Kalinichev et al., 2000; Wang et al., 2001; Kirkpatrick et al., 2005a,b,c).

Water and Cations in Smectite Interlayers

The group of clay minerals known as smectites (swelling clays) have smaller permanent negative structural (layer) charges than micas, and in the presence of water their interlayer galleries can expand and exchange cations with bulk solution. Because smectites are very common in soils, sediments, and sedimentary rocks and are also industrially important, their properties and behavior have received considerable attention for many decades. Many of the early NMR and computational studies of clay minerals focused on smectite swelling and interlayer structure and dynamics (see Morrow et al., 2013, for a comprehensive summary of the literature). Weiss et al. (1990), for instance, used ^{133}Cs NMR to demonstrate the effects of water content and temperature on cation dynamics in smectites and the capability of NMR methods to effectively probe cation structure and dynamics in these materials. The results show that in dehydrated hectorite (a very low Fe trioctahedral smectite mineral with structural charge

development dominated by Li^+ for Mg^{2+} substitution in the octahedral sheet) Cs^+ occurs on two sites, probably in 9 and 12 coordination by the basal oxygens of the clay, and that there are no discernable dynamical effects. These two sites result from the collapse of turbostratically disordered T-O-T layers around Cs^+, which readily sheds its hydration shell in favor of direct cation-surface oxygen interactions when equilibrated at low H_2O activity as a result of its low charge density. In contrast, for Cs-hectorite hydrated at 100% relative humidity (R.H.) or in slurries with CsCl solution, there are multiple hydrated Cs^+ structural environments, and dynamical effects are important. For the slurries there are two peaks near room temperature representing Cs^+ in bulk solution (the very narrow peak near 7.4 ppm) and Cs^+ associated with the clay (the broader peak near -11.9 ppm; Figure 1). At low temperatures, however, the peak for the Cs associated with the clay resolves into two peaks (Figure 1), a more negative one at – 29.8 ppm representing inner sphere coordinated Cs on the clay and a more positive one at 26.0 ppm representing outer sphere coordinated Cs on the clay. There is no peak for Cs^+ in bulk solution because the bulk H_2O domains have crystallized into ice-h. The 100% R.H. samples show generally similar behavior. Calculations using a well-established two-site exchange model show that the two Cs^+ peaks present at low temperature coalesce into the single peak at -11.9 ppm at site exchange frequencies of the order of 3 kHz in the -20 to -50^{o}C temperature range for the slurry samples. Overall, these results illustrate the important general point that the relatively weak bonding interactions among the clay layers, the exchangeable cations, and the water molecules allow for observable dynamical behavior at room temperature due to mutual and cooperative motion of the cations and coordinating water molecules. This behavior is in contrast to the dehydrated state where interlayer cations are coordinated only by the basal oxygens of the clay layers, and there is no detectable dynamical behavior at room temperature.

Early molecular simulations of smectite interlayers focused on the coordination environments of cations and water molecules in dry and hydrous interlayers, the energetics of interlayer expansion due to hydration, and the diffusional dynamics of interlayer species. For instance, Smith (1998) used Monte Carlo methods to investigate the structural and energetic effects of hydration of Cs montmorillonite with both tetrahedral and octahedral charge development. The results confirmed the presence of 9 and 12 coordinate Cs^+ in dehydrated smectite inferred from the NMR results of Weiss et al. (1990) and also showed the presence of both inner sphere and outer sphere coordinated Cs^+ for hydrous samples as also suggested by the NMR results. They also provided molecular scale understanding of the relationships between the interlayer water content, layer spacing and hydration energy; and provided a molecular scale picture of the interlayer structure at different hydration states. Ngouana and Kalinichev (2014) have recently performed a detailed MD study of the interlayer structure and dynamics for new, more realistically disordered models of Cs-montmorillonite that confirm the earlier findings. The use of the CLAYFF force field allowed them to also quantify the correlation of the Cs^+ surface sites with the Al/Si tetrahedral substitutions in the clay layers.

Many more recent MD simulations of smectite interlayers containing a variety of exchangeable cations at a range of hydration states have added significant dynamical information. The results confirm that cation diffusion and site hopping do not occur in fully dehydrated interlayers, because of coordination to the basal oxygens. This conclusion is in agreement with the ^{133}Cs NMR results of Weiss et al. (1990) and with more recent ^{23}Na, ^{39}K, and ^{43}Ca NMR results (Bowers et al., 2008a; 2011; 2014b). In interlayers hydrated to one water layer or more, however, the MD simulations show that both the cations and water diffuse at observable rates (e.g., Marry et al., 2011; Morrow et al., 2013; Ngouana and Kalinichev, 2014). For

instance, for Na-hectorite near room temperature the calculated diffusion coefficients for Na^+ are of the order of 10^{-7} cm^2s^{-1} for the 1 water layer hydrate and 10^{-6} cm^2s^{-1} for the 2 water layer hydrate (Morrow et al., 2103). The values for water are 2 – 3 times faster than for Na^+. The Na^+ and H_2O diffusion rates for the 2 layer hydrate are only about an order of magnitude less than in bulk solution. Similar trends are observed for Cs-montmorillonite (Ngouana and Kalinichev, 2014). The calculated values for the clays confirm the interpretation that the line narrowing in ^{23}Na, ^{39}K, ^{43}Ca, and ^{133}Cs NMR spectra of smectites observed near room temperature is due to rapid dynamical exchange of the cations and water molecules among different sites in the interlayers.

Recent experimental and computational results for Na-hectorite illustrate the direct, quantitative insight into cation and $^1H/^2H$ NMR results that MD simulations can provide (Ferrage et al., 2011; Bowers et al., 2011; Morrow et al., 2013). The variable temperature ^{23}Na NMR spectra of a deuterated 1.5:1.0 by weight ^2H_2O:Na hectorite paste are dominated by a resonance that is broad at -80°C, becomes progressively narrower with increasing temperature, and achieves a narrow, solution-like peak width near -20°C (Figure 2). As for the ^{133}Cs NMR results of Weiss et al. (1990), this behavior represents dynamical averaging of static disorder and second order quadrupolar line broadening due to progressively more rapid dynamics with increasing temperature. In contrast, the room temperature ^{23}Na spectrum of a sample that was dried over P_2O_5 and has little interlayer water shows a more complicated line shape due to lack of dynamical averaging of the second order quadruple interactions. For a sample that is dominantly a 2 water layer hydrate (labeled low H_2O in Figure 2) the resonance also shows a second order quadrupolar line shape demonstrating at most partial dynamical averaging of this interaction in hydrated interlayers. The less negative peak position for this resonance relative to that for the

dry sample may be due to a reduced second order quadrupolar interaction due to partial dynamic averaging when H_2O is present. Isotropic averaging is not expected in the interlayer gallery even with water present, because of the electric field gradient due to the parallel clay layers. As discussed above, MD simulations of Na^+ in hydrated hectorite interlayers show rapid diffusional motion of Na^+ and H_2O among generally similar interlayer sites, consistent with such dynamical averaging .

^2H NMR is often useful for investigating the dynamics of water molecules in many materials and is particularly effective in clay minerals where the basal surface provides an important reference for understanding the motion. ^2H has nuclear spin 1, and the spectra consist of overlapping signal from the -1,0 and 0,1 transitions that generate the classic Pake doublet pattern in the absence of isotropic dynamical averaging. The ^2H peak shape and width are very sensitive to the symmetry and rate of motion of the ^2H_2O molecules and their orientation with respect to the basal surface, providing otherwise unobtainable insight into the ^2H_2O structural environment and dynamics. For the Na-hectorite paste, the ^2H NMR spectra at temperatures below -30^{o}C contain two Pake doublets, a relatively narrow one due to unfrozen, anisotropically dynamically averaged water molecules associated with the smectite surface and a broader one due to ice-1h. The relative intensity of the ice resonance decreases in intensity with increasing temperature due to an increased rate of ^2H tetrahedral jump motion within the crystal lattice (Bowers et al, 2011: Figure 3, left side). The water molecules associated with the clay are best thought of as being principally on exposed basal surfaces, because Na-hectorite expands osmotically, disaggregating into individual T-O-T layers or small packets of such layers in the presence of excess water (more than required to produce a 2 layered hydrate). The Pake doublet for it narrows progressively with increasing temperature due to dynamical averaging of

molecules between the surface sites and bulk water, which has a very narrow peak due to isotropic averaging. The ^2H spectra of the sample with dominantly 2 water layers (Figure 3 right side) contain a single Pake doublet with a slightly larger splitting of the singularities than for the paste sample. This resonance represents interlayer water molecules undergoing anisotropic dynamic averaging in the interlayer galleries. The splitting of the singularities is temperature invariant, because all H_2O molecules are in the interlayer or associated with external surfaces at all times due to a lack of bulk H_2O domains with which to exchange, and because dynamical effects average the NMR signal to the same line shape as long as the frequency of the process is greater than approximately an order of magnitude larger than the static line width. Here the peak width is of the order of 10^4 Hz. Rotational frequencies for water molecules in solution are typically of the order of 10^{12} Hz, and the results here show that this frequency is at least 10^5 Hz for the interlayer and surface H_2O molecules throughout the observed temperature range. Deuterated K-exchanged hectorite shows similar behavior (Bowers et al., 2008).

Modeling of the ^2H spectra for the two water layer Na hectorite assuming a 2-component, constrained rotational mechanism of motion termed the fast limit C_2/C_3 model generates line shapes that agree very well with the experimental results (Bowers et al., 2011; Figures 4 and 5). To our knowledge no other model of ^2H_2O reorientation does this, including the tetrahedral jump model that describes the behavior of ice-1h (Wittebort, et al. 1998). The 2-component constrained rotation model assumes rapid hopping of the interlayer water molecules among sites with C_3 symmetry around the normal to the basal surface combined with rotation of the water molecules around their C_2 (dipole) axis at frequencies at least an order of magnitude faster than the site hopping. Thus, the model and NMR spectra together constrain the rate of C_3 reorientation to being between 10^4 and 10^{11} Hz. The calculated spectra also depend very

sensitively on the angle between the normal to the basal smectite surface and the C_2 rotation axis (ω in Figure 5). For this sample, the calculated spectra match the observed spectra well when the mean ω value is either 51° or 59°. These values can be thought of as representing stretched or compressed octahedral orientation of water molecules with respect to the basal surface, respectively, and are essentially symmetrical with respect to the ideal octahedral angle of 54.7°. At this ideal angle the quadrupolar coupling is 0, and the resonance would be a narrow singlet. The MD simulations for 2 water layer Na-hectorite hydrate resolve the uncertainty in the ω angle (Morrow et al., 2013). In these simulations, the average ω value is 51-53°, showing that the interlayer water undergoes hopping among sites with an average orientation more stretched than the ideal octahedral angle.

Little is known about the detailed energetics of site hopping in smectite interlayers, and the computational approach known as metadynamics has the potential to add considerably to this understanding. The metadynamics simulation algorithm (see, e.g., Ensing et al., 2006) uses the same force field approach as classical MD, but adds additional biasing forces to progressively drive the system over an activation barrier in a prescribed direction (the collective variable). Defining this collective variable in an effective way is critical, and knowing the interlayer structure for smectites from the MD simulations allows us to do so. For 2 water layer Na-hectorite, a useful collective variable to probe H_2O dynamics around Na is the angle θ between the normal to the smectite surface and the Na-O_{H2O} vector for those water molecules coordinated to Na (Figure 5). As discussed above, at this hydration state, Na occurs on outer sphere sites and is 6-coordinate by H_2O. The metadynamics results show that energy minima occur at θ values near 50° and 124° for the two layers, which are comparable to the ω value of 51-53° obtained for all water molecules from the MD simulation. The metadynamics results also show that the

activation energy for H_2O to hop between the two water layers (that is, between sites coordinated to the basal surface on either side of the interlayer, corresponding to the θ values near 50^o and 124^o) is 3.3 kJ/mol. The thermal energy at room temperature is ~2.5 k/mol, sufficient to often overcome this activation barrier and consistent with the relatively large calculated diffusion coefficients and the observed NMR line narrowing

Solute Interaction with Natural Organic Matter

The interaction of dissolved aqueous species with natural organic matter (NOM) such as humic substances can significantly influence their geochemical fate and transport behavior (e.g., Tipping, 2002), but the molecular scale processes controlling these interactions are poorly understood. Individual NOM molecules have molecular weights of hundreds to thousands of Daltons and their interaction with water molecules and small dissolved species can be investigated by NMR and MD methods in ways similar to those used for mineral-fluid interactions. ^{133}Cs and ^{35}Cl NMR data for dissolved Suwannee River NOM in CsCl solutions and parallel MD simulations of the interaction of Cs^+ and Cl^- with a model NOM molecule illustrate the effectiveness of the combination of these two methods (Xu et al., 2006). The NMR data were collected at pHs from 3.4±0.5 to 9.0±0.5 and CsCl solution concentrations from 10^{-4} to 4M. The MD simulations used the TNB (Temple-Northeastern-Birmingham) NOM model (Davies et al., 1997; Sein et al., 1999) with its three carboxylic sites deprotonated and all other R-OH and amine groups protonated, simulating near-neutral pH conditions. The NMR results show that at all pHs for a given CsCl concentration the presence of dissolved NOM does not affect the ^{35}Cl chemical shifts and T_1 relaxation rates or the ^{133}Cs chemical shifts. The ^{133}Cs T_1 relaxation rates, however, increase greatly with increasing pH and decreasing CsCl concentration (Figure 6), demonstrating substantial interaction of Cs^+ with the NOM. T_1 relaxation must be

stimulated by processes with components in their dynamical power spectra (spectral density functions) at the NMR resonance (Larmor) frequency. Interaction with surfaces or bound sites increases the T_1 relaxation rates, because the typical correlation times for ion-H_2O interactions in bulk solution are of the order of 10^{10} Hz, and the decreased rates of motion near the surface increase the intensity of the power spectrum at the Larmor frequency (here 78.67 MHz). The presence of only one resonance for each sample, however, demonstrates that there is exchange of Cs^+ between the bulk solution and near-surface sites at frequencies in the kHz range or faster. pH dependent negative structural charge development on Suwannee River NOM is related principally to deprotonation of carboxylic groups (pK_a near 4) and phenolic and amine groups (pK_as near 9). Thus, the increasing ^{133}Cs T_1 relaxation rates with increasing pH are due to progressively increasing interaction with these functional groups as they become deprotonated. The increasing T_1 rates with decreasing CsCl concentration is due to a progressively larger fraction of the Cs interacting with the NOM.

The question is then, what is the nature of this interaction? The absence of an effect of NOM on the ^{133}Cs chemical shift suggests that the local coordination environment of Cs^+ is essentially the same when it is in bulk solution and interacting with the NOM. The NOM-Cs^+ MD models show that Cs^+ is associated principally with the deprotonated carboxylic groups and almost exclusively as outer sphere complexes with, on average, 8 NN H_2O molecules, 0.3 O-atoms from the $–COO^-$ groups and even less coordination by R-OH groups. In the NNN shell there are ~40 H_2O molecules and 1 O of $–COO^-$ (Xu et al., 2006). This coordination environment is very similar to that in bulk solution at low CsCl concentrations, resulting in similar chemical shifts. The MD simulations show that Cs and Cl diffuse rapidly with NOM present, confirming the conclusion that the rate of exchange of Cs between bulk solution and sites on the NOM is

very rapid. Diffusion coefficients for Cs^+ calculated from the MD simulations of NOM with Cs^+ concentrations from 0.3M (only the minimum Cs^+ needed to charge balance the $–COO^-$ sites) to 4M and for the bulk solution without NOM are all of the order of 10^{-5} cm^2s^{-1}, similar to values in bulk aqueous solutions The MD simulations also show little effect of the presence of NOM on the low frequency (0 – 50 cm^{-1}; ~10^{11} – 10^{12} Hz) translational power spectrum of Cs. The simulations also show that Cl does not associate with the NOM molecule in any way, consistent with the absence of any effect of NOM on the ^{35}Cl NMR behavior.

Interaction of Clays, Organic Matter and CO_2

Clay minerals and NOM are well known to form composite materials, and these composites are thought to play significant roles in controlling the transport and fate of many chemical species in low temperature geological environments and in C-sequestration situations. The molecular scale processes controlling clay-organic interaction have been less well studied than clays by themselves (e.g., Siantar et al., 1994), but the combination of NMR and MD calculations can provide the same types of structural, dynamic, and energetic information (see Greathouse, et al., 2014, for recent discussion). This section summarizes recent modeling and NMR work on the interaction of CO_2 with clays and clay-organic materials. This interaction is of potential importance for geological CO_2 sequestration and potentially the capture of CO_2 by soils at near-surface geochemical conditions.

MD calculations of the interaction of NOM and its interaction with smectites predate NMR experiments with this type of system (Sutton and Sposito, 2005, 2006; Sutton et al., 2005) and played a central role in defining the nature of the interactions that lead to clay-organic binding. Their results for Ca-montmorillonite show that at pHs less than the pKa of the carboxylic groups of NOM (ca. pH = 4) the binding is controlled dominantly by hydrophobic

436 interactions, in which the hydrophobic regions of the NOM cluster together and approach the
437 clay surface to minimize NOM interaction with water molecules. In contrast, at pHs above the
438 pKa of the carboxylic groups, Ca^{2+} acts as a partially hydrated cation bridge between the NOM
439 and clay surface by coordinating to both the $–COO^-$ group and the surface. The Ca^{2+} ions adopt
440 a coordination environment that is either inner-sphere with the clay surface and outer-sphere
441 with the NOM functional group or that is outer-sphere with the clay surface and inner-sphere
442 with the NOM functional group. There would presumably be similar interactions involving
443 deprotonated phenolic and amine sites at pHs larger than their pK_as of ~ 9.

444 Experimental studies have shown that CO_2 can be intercalated in smectite interlayers
445 (e.g., Fripiat et al., 1974; see Cygan et al., 2012, and Bowers et al., 2014a for summaries), and
446 recent MD modeling of the interaction of montmorillonite and hectorite with CO_2 provide a
447 molecular scale picture of the structure. Botan et al. (2010) used molecular simulation methods
448 to show that Na-montmorillonite with several different interlayer water contents preferentially
449 incorporates CO_2 in its interlayer galleries relative to CO_2-saturated water at 75°C and 25 and
450 125 bar, particularly in the one-layer hydrate. Cygan et al. (2012) developed fully flexible force
451 field parameters for CO_2 that are compatible with the CLAYFF force field. Using this force field,
452 they showed that interlayer confinement causes a blue-shift of the frequency of the CO_2 bending
453 mode but does not substantially affect the asymmetric stretching mode, in agreement with
454 experimental results. Further MD simulation of the montmorillonite-CO_2 system using the same
455 force field showed that in a system with just one interlayer CO_2 layer the C_{CO2} occur in the mid-
456 plane of the interlayer, that in the absence of H_2O the Na interacts with the O_{CO2}, and that there is
457 dynamical correlation between Na site hopping and CO_2 reorientation between an orientation
458 parallel to the basal surface and with a distribution of angles relative to it (Krishnan et al., 2013).

NMR data collected using a novel high-pressure MAS sample probe (Hoyt 2011) is now beginning to provide structural and dynamical data for interlayer species in clay-CO_2 systems at reservoir conditions. ^{13}C spectra of a one-layer hydrate of Ca-montmorillonite acquired at 50°C and 90 bar CO_2 pressure show a substantially increased line width relative to supercritical CO_2 under the same conditions, demonstrating CO_2-clay interaction. *In situ* XRD data for the same sample shows increased basal spacing, and together these data strongly suggest that CO_2 is incorporated into the interlayer (Loring, et al., 2012). In contrast, the $^{13}CO_2$ line width for kaolinite under the same conditions does not increase. Kaolinite does not have expandable interlayer galleries, demonstrating that interaction of CO_2 with only external silicate surfaces does not cause the observed line broadening. The spectra for both Ca-montmorillonite and kaolinite contain only one resonance, which is at the same chemical shift as CO_2, demonstrating, that at least in these experiments it did not react to form a carbonate species.

Bowers et al. (2014a) also observed broadening of the $^{13}CO_2$ resonance at 90°C and 50 bar CO_2 pressure for Na-hectorite, consistent with CO_2 incorporation in the interlayers. This sample had been equilibrated at room humidity, but the extent of interlayer hydration after equilibration with supercritical CO_2 is unknown. They also acquired ^{23}Na NMR spectra for the base Na-hectorite and ^{13}C and ^{23}Na NMR spectra for a composite of the Na-hectorite and Suwannee River humic acid (HA). These ^{13}C spectra show a progressive increase in the width of the $^{13}CO_2$ resonance from a supercritical CO_2 blank to the Na-hectorite to the composite, indicating progressively increasing interaction of the CO_2 and solids. XRD showed that this sample had substantial HA in the interlayers, and the results are consistent with increased CO_2 incorporation in the interlayers in the presence of organic matter. Again, there was no change in the $^{13}CO_2$ chemical shift that would indicate reaction of CO_2 to carbonate species.

482 CO_2 has little effect on the ^{23}Na chemical shift in the base Na-hectorite but increases the
483 signal intensity by ~23% (Figure 7) and also increases the ^{23}Na T_1 relaxation rates. The increased
484 signal intensity is consistent with an increase in the rate of Na^+ motion causing an increase in the
485 amount of signal from the ±1/2,±3/2 satellite transitions observed with central -1/2,+1/2 central
486 transition peak. The increased relaxation rates reflect increased intensity in the power spectrum
487 at the Larmor frequency, as for the NOM in solution discussed above. For ^{23}Na in the composite,
488 CO_2 increases the peak area by about 30%, increases the T_1 relaxation rates, and also changes the
489 peak maximum by ~ 7 ppm to less negative values. This latter change clearly demonstrates the
490 presence of CO_2 in the interlayer galleries. Thus, the data also show that HA is not a barrier to
491 the uptake of CO_2 by the clay and that CO_2 stimulates more rapid Na^+ motion in both base
492 smectites and smectite-organic matter composite materials.
493 Computational modeling of Na-montmorillonite with interlayer (poly)ethylene glycol
494 (PEG) provides insight into how organic molecules interact with smectite surfaces, charge
495 balancing cations and CO_2 (Krishnan et al., 2013). The monomeric unit of PEG ($-CH_2OCH_2-$)
496 consists of two methylene groups connected by an ether oxygen that plays an important role in
497 the interactions with the cations. The MD results for the montmorillonite-CO_2 system show that
498 all the Na^+ ions are coordinated to the basal surface but are also coordinated to the O_{CO2}. In
499 contrast, in the montmorillonite-PEG and montmorillonite-PEG-CO_2 systems many Na^+ ions are
500 displaced from the surface and are coordinated by the O_{PEG} and to a much smaller extent by the
501 O_{CO2}. The presence of CO_2 in the montmorillonite-CO_2 system enhances Na^+ diffusion through
502 cooperative motion of the cation and the CO_2 molecules. This result is in agreement with the
503 increased rate of Na^+ motion in the presence of supercritical CO_2 proposed by Bowers et al.
504 (2014a) based on the *in situ* high pressure NMR results described above. Structurally, the results

505 show that the coordination of CO_2 occurs principally through interaction of the C_{CO2} with the
506 O_{CO2} and O_{PEG} in an arrangement very similar to that in supercritical CO_2 (Figure 8). This
507 arrangement suggests that the dry ice structure (Suzuki and Schnepp, 1971) is a useful model for
508 understanding CO_2 in mineral systems in a way analogous to the relationship between the ice 1h
509 and water structures.

510 **Layered Double Hydroxides**

511 The interlayer structure, dynamics and energetics of LDHs are controlled by the
512 electrostatic attraction between the exchangeable anions and the negatively charged hydroxide
513 layers, H-bond donation from the structural hydroxide sites to the interlayer anions and O_{H2O},
514 and the mutual interaction among the interlayer species including H-bond donation from the
515 water molecules to the anions and electrostatic repulsion among the anions (e.g., Wang, et al.,
516 2001). Because of their typically high layer charge, most LDHs do not expand beyond 1 or 2
517 water layers, but as for smectite interlayers development of an integrated H-bond network is an
518 essential part of minimizing the interlayer energy.

519 The mineral hydrocalumite (also known as Friedel's salt, nominally
520 $[Ca_2Al(OH)_6]Cl{\cdot}2H_2O$, has a well ordered Ca/Al distribution in the hydroxide layer and a quite
521 well ordered arrangement among the Cl and H_2O in the interlayer. Because of this, it is one of
522 the few LDHs for which the full crystal structure is known (Terzis et al., 1987). This phase is of
523 particular importance in the chemistry of Portland cement.

524 Hydrocalumite undergoes a structural phase transition from a low-temperature phase with
525 C2/c symmetry to a high temperature phase with R-3c symmetry at about 35^{o}C due to
526 displacement of the Cl^- and H_2O in the interlayer (Rapin et al., 2002; Andersen et al., 2002). In
527 the high temperature phase, the Cl^- is at the center of a trigonal antiprism formed by six water

molecules and also accepts H-bonds from 6 structural OH groups. In the low temperature phase (see also Terzis et al., 1987) the Cl^- is in distorted 10-coordinate sites with four NN H_2O and six NN structural OH groups, with two additional H_2O at longer distances. This phase change is directly reflected in the static ^{35}Cl NMR spectra as a change from a quadrupolar line shape with triaxial symmetry at low temperatures (reflecting the distorted Cl^- site) to one with uniaxial symmetry in the high temperature phase, reflecting the trigonal coordination environment (Figure 9; Kirkpatrick et al., 1999). The phase transition for the NMR sample probably occurs at a lower temperature than reported for the diffraction results because of the presence of impurity CO_3^{2-}. In both the low temperature and high temperature phases, the water molecules have three NN H_2O molecules, leading to partial occupancy of the H-positions, because the H_2O molecules only have two H-bonds to donate. MD modeling of the low temperature structure shows that this partial occupancy occurs by dynamical libration (restricted rotational hopping) of the water molecules among the three possible orientations (Kalinichev, et al., 2000; 2010). This results in a time averaged uniaxial symmetry, in agreement with the NMR results. Computed power spectra of the motions of the interlayer species calculated as the Fourier transforms of the atomic velocity autocorrelation function show that the frequency of these librational motions are in the far IR range at less than 600 cm^{-1} (~ 10^{12}-10^{13} Hz). This frequency is much larger than the ~10^4 Hz frequencies needed to cause dynamical averaging of the ^{35}Cl NMR spectrum. If this dynamics were not occurring, the H-bond environment of the Cl^- would not be uniaxial, resulting in a triaxial ^{35}Cl powder pattern.

Unlike the ^2H NMR spectra of interlayer H_2O in smectite (Figure 3), the ^{35}Cl spectra of the high temperature phase of hydrocalumite become progressively narrower at temperatures above ~50°C. This is probably the result of partial averaging the of the time averaged quadrupole

coupling constant by relatively slow (frequencies of the order of kHz) diffusional hopping of the interlayer Cl^- and H_2O, which would mix signal with a near-zero QCC into the observed line shape. The MD simulations do not observe interlayer diffusion, but because of the limited time for which they could be run could only detect such motion if it were occurring at frequencies > ~10^{10} Hz. Motion at these frequencies would probably result in complete narrowing the of the ^{35}Cl NMR resonance due to isotropic averaging of the quadrupolar effects, as observed for the alkali metals in smectite interlayers.

LDHs can also develop positive structural charge by Li for vacancy substitution in the gibbsite structure, giving nominal compositions of $LiAl_2(OH)_6Cl{\cdot}nH_2O$, although many samples have Li contents slightly less than 1/formula unit. The $LiAl_2$ LDHs have wide ranging potential applications as catalysts, filtration and exchange materials, and in drug and gene-therapy delivery systems. MAS and static ^{35}Cl NMR data indicate that the Cl^- environments vary significantly with hydration state, and computational MD models provide molecular scale understanding of the origins of the structural, dynamical and energetic behavior of these materials (Hou, et al., 2002). Samples that have been fully dehydrated by heating at 200°C or being held over P_2O_5 yield a single ^{35}Cl NMR resonance that collapses to a single narrow resonance under MAS and in the static spectrum is dominated by chemical shift anisotropy with uniaxial symmetry (Figure 10e, 10f, 10m, 10i). This pattern is the result of the one, well ordered Cl^- position in the crystal structure of the fully dehydrated form (Besserguenev, 1997). In this structure, the Cl^- accepts six H-bonds from OH groups of the hydroxide layers, three from each side of the interlayer, and is located directly above and below the Li sites of the two adjacent hydroxides layers (Figure 11c). With increasing hydration, the relative intensity of this resonance decreases and the resonance becomes less well defined, indicating increasing disorder, and is progressively replaced by a

broad, featureless resonance. This broad resonance is not averaged by MAS (Figure 10c), indicating that it is dominated by inhomogeneous broadening due to structural disorder or dynamical effects, rather than CSA or quadrupolar effects. In variable temperature experiments with the paste sample, these two resonances merge with one another at about 70°C, indicating site exchange at frequencies of at least 10^4 - 10^5 Hz at this temperature (the observed static line widths are of the order of 10^4 Hz broad). For the paste there is also a narrow, solution-like resonance due to Cl^- on exterior surfaces that undergoes isotropic averaging due to exchange with the bulk solution but that does not exchange with the interlayer Cl^-. At low temperatures the two interlayer resonances merge into a broad peak that is skewed towards high field (more negative chemical shifts), the characteristic feature of second order quadrupolar effects that are averaged by dynamical processes.

The structure of hydrated $LiAl_2(OH)_6Cl{\cdot}nH_2O$ is not well known from diffraction experiments, although Rietveld refinement of powder XRD data indicate a disordered Cl^-/H_2O distribution (Besserguenev et al., 1997). MD simulations are consistent with the XRD structure for the dehydrated sample (Figure 11c) and for hydrated interlayers provide otherwise unobtainable structural, dynamical and energetic understanding (Hou et al., 2002). For the $LiAl_2(OH)_6Cl{\cdot}1H_2O$ composition, the MD simulations show a disordered but not random interlayer arrangement. The water molecules are located at the mid-plane of the interlayer, as also shown by the diffraction data (Besserguenev et al., 1997), and are predominantly located near the H atoms of the OH groups. The O atoms of the H_2O molecules on these positions receive two H-bonds, one each from an OH group on either side the interlayer. These water molecules are in a stable, distorted tetrahedral coordination (Figures 11) very similar to that in bulk liquid water. Because these H_2O molecules are predominantly in the mid-plane of the

interlayer, they can donate H-bonds to the Cl^-, all of which are also located at the mid-plane of the interlayer but with several different local structural environments. Some are similar to the sites in the dehydrated phase, although they are rarely exactly along the trans-interlayer Li-Li vector. Cl^- on these sites gives rise to the CSA dominated peak in the NMR spectra of the hydrated samples, and their disordered local bonding environments observed in the MD simulations gives rise to the experimentally observed decreased resolution of this peak for the hydrated samples. Other Cl^- atoms in the MD simulation occur between vacant tetrahedral sites of adjacent hydroxide layers and as for the first type of site are 6-coordinated by three OH groups from above and three from below and are in a trigonal prism arrangement.

Most of the Cl^- ions in the MD simulations, however, occur on distorted octahedral sites and receive two H-bonds from OH groups from the hydroxide layer on one side of the interlayer, two from OH groups from the other side, and one from each of two adjacent water molecules (Figure 11). This structural arrangement is quite similar to that of Cl^- in aqueous solution. Cl^- on these types of sites give rise to the broad, featureless NMR resonance that is not averaged by MAS. The MD results show that this behavior is due to inhomogeneous line broadening due to structural disorder that is not fully averaged by dynamic processes. The presence of the two observable resonances at room temperature shows that Cl^- is not exchanging among the different types of sites at frequencies larger than 10^4 - 10^5 Hz, and their merging near 70°C show that such exchange is occurring at that temperature. The MD simulations show Cl^- and H_2O site hopping at $\sim 10^8$ and 10^9 Hz, respectively, although the frequencies are at the limits of observability in the 100 ps duration of the simulations. The poor resolution between the two NMR resonances and quadrupolar contributions to the line shape at temperature less than -30°C shows that the vibrational and translational atomic motions giving rise to the room temperature line shapes slow

620 to frequencies less than ~ 10^4 Hz near -30°C. This is the same temperature range at which line
621 broadening begins to occur with decreasing temperature for interlayer cations in clays, consistent
622 with the dominance of electrostatic and H-bonding in the interlayer environments in clays and
623 LDHs. The MD results also show the expected rapid (ca. 10^{11} Hz) restricted, librational hopping
624 of the water molecules among different H-bond orientations, as observed in clay interlayers. This
625 librational motion is expected to occur at all temperatures observed in the NMR experiments,
626 and changes in its frequency probably do not affect the observed line shapes. It is important to
627 keep in mind that the melting point and the critical point of the SPC (simple point charge) water
628 model used in our MD simulations are located ~80° and ~30° , respectively, below their
629 experimental values (Vega et al., 2005; Kalinichev, 2001). Thus, the P-T phase diagram of the
630 simulated water has to be properly scaled in order to obtain a correct comparison with the
631 experimentally observed structural and dynamic molecular behavior.
632 The simulations also provide structural understanding of the smaller interlayer
633 water content of the $LiAl_2$ LDH phases compared to the Ca_2Al (hydrocalumite) and $Mg_{3-x}Al_x$
634 LDH phases known as hydrotalcite. For hydrocalumite, the maximum H_2O/Cl^- ratio is 2, because
635 the interlayer O_{H2O} coordinate the Ca of the hydroxyl layer and thus form two sublayers on either
636 side of the mid-plane of the interlayer. Thus, at any instant the $Cl^-$are 10 coordinate (six OH and
637 four water molecules), and there is a stable but dynamic H-bonding network with the H-bonds
638 from the OH groups given predominantly to the Cl^-. MD modeling of the Cl-Mg,Al LDH
639 suggests a similar but less ordered arrangement with at least some of the O atoms of water
640 molecules coordinating Mg (Wang et al., 2001). In contrast, in the $LiAl_2$ phases the O_{H2O} do not
641 coordinate either Li or Al in the hydroxide layer, and of the six OH groups per formula unit, two
642 donate H-bonds to a H_2O and four to a Cl^-. Thus, there are no stable sites for substantial amounts

643 of additional water beyond the 1/1 H_2O/Cl^- ratio. The similarity of the Cl^- and H_2O bonding
644 environments in the $LiAl_2$ LDHs to those in bulk water are consistent with the stability of the
645 computed arrangement, and in an MD simulation $LiAl_2$ LDH with a H_2O/Cl ratio of 2/1, the
646 structure disaggregated.

647 Like alumino-silicate clay minerals, LDH phases readily interact with organic molecules.
648 Because of the positive layer charge of LDHs, this interaction is not mediated by cations, and
649 anionic organic species of many types can be readily intercalated in the interlayer galleries. ^{13}C
650 NMR results for citrate hydrotalcite (the Mg,Al LDH) show that the citrate molecules have the
651 same chemical shifts in the interlayer as in solution, indicating only electrostatic interaction with
652 the hydroxide layers and that grafting to the hydroxide layers does not occur (Li and Kirkpatrick
653 2007). The ^{13}C MAS NMR peak widths and signal/noise ratios in the ^{1}H-^{13}C cross polarization
654 MAS NMR spectra decrease in parallel with increasing basal layer spacing as the water content
655 increases (8.9 Å at 0% R.H. to 18.9 Å at 100% R.H.). These observations demonstrate
656 increasingly rapid dynamical disorder with increasing water content, as is also observed for
657 alkali metals in smectites (discussed above).

658 MD simulations of citrate hydrotalcite support these interpretations and as for alumino-
659 silicate clays provide a more detailed molecular scale picture (Kumar et al., 2006). The results
660 show that citrate-hydrotalcite has a strong thermodynamic affinity for water up to large hydration
661 levels, in contrast to LDHs containing small inorganic anions. This result is consistent with the
662 observed increase in basal spacings with increasing R.H. The MD results suggest that this
663 expansion occurs because citrate anions prefer to receive H-bonds from water molecules rather
664 than the basal OH groups to allow for the formation of an integrated H-bond network in the
665 interlayer gallery. In parallel the citrate ions change orientation from dominantly parallel to the

basal surfaces to dominantly perpendicular to them with increasing water content, again to allow for a more integrated H-bond network.

Implications

The interactions among minerals, inorganic cations and anions, organic species and geological fluids play central roles in many geochemical processes. Many of these interactions are dominated by Coulombic, H-bond, and van der Waals interactions, resulting in statically and dynamically disordered systems and molecular scale processes with characteristic room-temperature frequencies varying from at least as small as 10^2 Hz to > 10^{12} Hz. The examples of combined experimental NMR spectroscopy and computational molecular-scale modeling studies reviewed in this paper illustrate how these methods can provide otherwise unobtainable structural, dynamical and energetic information about mineral-fluid systems. In combination with the wide range of other experimental and computational tools that have become available in the past few decades, this approach will continue to play an important role in understanding such systems at geological conditions from the earth's surface (or the surfaces of other planets) to deep into the interior. Continued development of experimental methods and force fields for computation appropriate to elevated pressures and temperature s will be an ongoing challenge (e.g., Stefánsson et al., 2013).

Acknowledgements

Much of our research integrating experimental NMR and computational MD modeling described here was supported by the U. S. Department of Energy Basic Energy Science Geosciences Program, most recently grants DEFG02-10ER16128 and DE-FG02-08ER15929. We are very grateful for this support. Some of the NMR results were obtained using facilities

689 housed at the Environmental Molecular Sciences Laboratory, a national scientific user facility
690 sponsored by the Department of Energy's Office of Biological and Environmental Research and
691 located at Pacific Northwest National Laboratory (PNNL). The supercomputing resources of the
692 NSF TeraGrid and XSEDE and of the US DOE National Energy Research Scientific Computing
693 Center (NERSC) were used for some of the simulations. Many students and post-doctoral
694 fellows contributed greatly to this work, including Charles A. Weiss, Jr.; Younjoun Kim; Jianwei
695 Wang; Xiaoqiang Hou; Xiang Xu; Marc Reinholdt; P Padma Kumar; Qiang Li; Eugenia
696 Iskrenova-Tchoukova; Brennan O. Ferguson; Arielle Polakos; and Jared W. Singer. We also
697 gratefully acknowledge the collaboration of Randall T. Cygan and Jeffrey Greathouse (Sandia
698 National Laboratories); David L. Bish (Indiana University); and David W. Hoyt, Sarah D.
699 Burton, Tamas Varga, Mark Bowden, and Bruce Arey (Pacific Northwest National Laboratory).
700 The manuscript benefited considerably from the suggestions of two anonymous reviewers.

701

References Cited

Aicken, A.M., Bell, I.S., Coveney, P.V., and Jones, W. (1997) Simulation of layered double hydroxide intercalates. Advanced Materials, 9(6), 496-500.

Alder, B.J., and Wainwright, T.E. (1959) Studies in molecular dynamics .1. General method. Journal of Chemical Physics, 31(2), 459-466.

Allen, M.P., and Tildesley, D.J. (1987) Computer Simulation of Liquids, 385 p. Oxford University Press, New York.

Andersen, M.D., Jakobsen, H.J., and Skibsted, J. (2002) Characterization of the alpha-beta phase transition in Friedels salt ($Ca_2Al(OH)_6Cl{\cdot}2H_2O$) by variable-temperature ^{27}Al MAS NMR spectroscopy. Journal of Physical Chemistry A, 106(28), 6676-6682.

Bailey, S. W., ed. (1988) Hydrous phyllosilicates (exclusive of micas). Reviews in Mineralogy, 19, 725 p. Mineralogical Society of America, Washington D.C.,

Besserguenev, A.V., Fogg, A.M., Francis, R.J., Price, S.J., Ohare, D., Isupov, V.P., and Tolochko, B.P. (1997) Synthesis and structure of the gibbsite intercalation compounds $[LiAl_2(OH)_6]X$ {X=Cl, Br, NO_3} and $[LiAl_2(OH)_6]Cl \cdot H_2O$ using synchrotron X-ray and neutron powder diffraction. Chemistry of Materials, 9(1), 241-247.

Bloch, F., Hansen, W. W., and Packard M. (1946) Nuclear induction. Physics Review, 69, 127.

Boek, E.S., Coveney, P.V., and Skipper, N.T. (1995) Monte Carlo molecular modeling studies of hydrated Li-, Na-, and K-smectites: Understanding the role of potassium as a clay swelling inhibitor. Journal of the American Chemical Society, 117(50), 12608-12617.

Botan, A., Rotenberg, B., Marry, V., Turq, P., and Noetinger, B. (2010) Carbon dioxide in montmorillonite clay hydrates: Thermodynamics, structure, and transport from molecular simulation. Journal of Physical Chemistry C, 114(35), 14962-14969.

Boutton, T.W., Archer, S,R, Midwood, A,J, Zitzer, S,F, and Bol, R. (1994) $\delta^{13}C$ values of soil organic carbon and their use in documenting vegetation change in a subtropical savanna ecosystem. Geoderma, 82 (1-3) 5-41.

Bowers, G.M., Bish, D.L., and Kirkpatrick, R.J. (2008a) H_2O and cation structure and dynamics in expandable clays: ^{2}H and ^{39}K NMR investigations of hectorite. Journal of Physical Chemistry C, 112(16), 6430-6438.

Bowers, G.M., Bish, D.L., and Kirkpatrick, R.J. (2008b) Cation exchange at the mineral-water interface: H_3O^+/K^+ competition at the surface of nano-muscovite. Langmuir, 24(18), 10240-10244.

Bowers, G.M., Hoyt, D.W., Burton, S.D., Ferguson, B.O., Varga, T., and Kirkpatrick, R.J. (2014a) In situ ^{13}C and ^{23}Na magic angle spinning NMR investigation of supercritical CO_2 incorporation in smectite - natural organic matter composites. Journal of Physical Chemistry C, 118(7), 3564-3573.

Bowers, G.M., Singer, J.W., Bish, D.L., and Kirkpatrick, R.J. (2011) Alkali metal and H_2O dynamics at the smectite/water interface. Journal of Physical Chemistry C, 115(47), 23395-23407.

Bowers, G.M., Singer, J.W., Bish, D.L., and Kirkpatrick, J. (2014b) Structural and dynamical relationships of Ca^{2+} and H_2O in smectite / $^{2}H_2O$ systems. American Mineralogist, 99(2-3), 318-331.

Brindley, G. W., and Brown, G. (1980) Crystal structures of clay minerals and their X-ray identification, 495 p. Mineralogical Society Monograph No.5, Mineralogical Society, London.

Cadars, S., Layrac, G., Gerardin, C., Deschamps, M., Yates, J.R., Tichit, D., and Massiot, D. (2011) Identification and quantification of defects in the cation ordering in Mg/Al layered double hydroxides. Chemistry of Materials, 23(11), 2821-2831.

Cadars, S., Guegan, R., Garaga, M.N., Bourrat, X., Le Forestier, L., Fayon, F., Huynh, T.V., Allier, T., Nour, Z., and Massiot, D. (2012) New insights into the molecular structures, compositions, and cation distributions in synthetic and natural montmorillonite clays. Chemistry of Materials, 24(22), 4376-4389.

Chang, F.R.C., Skipper, N.T., and Sposito, G. (1997) Monte Carlo and molecular dynamics simulations of interfacial structure in lithium-montmorillonite hydrates. Langmuir, 13(7), 2074-2082.

Cygan, R.T, (2001) Molecular modeling in mineralogy and geochemistry. Reviews in Mineralogy, 42, 1-30.

Cygan, R.T., Greathouse, J.A., Heinz, H., and Kalinichev, A.G. (2009) Molecular models and simulations of layered materials. Journal of Materials Chemistry, 19(17), 2470-2481.

Cygan, R.T., and Kubicki, J.D. (2001) Molecular Modeling Theory: Applications in the Geosciences. 531 p. Reviews in Mineralogy and Geochemistry, 42, Geochemical Society and Mineralogical Society of America, Washington D.C.

Cygan, R.T., Liang, J.J., and Kalinichev, A.G. (2004) Molecular models of hydroxide, oxyhydroxide, and clay phases and the development of a general force field. Journal of Physical Chemistry B, 108(4), 1255-1266.

Cygan, R.T., Romanov, V.N., and Myshakin, E. (2012) Molecular simulation of carbon dioxide capture by montmorillonite using an accurate and flexible force field. Journal of Physical Chemistry C, 116(24), 13079–13091.

769 Davies, G., Fataftah, A., Cherkasskiy, A., Ghabbour, E.A., Radwan, A., Jansen, S.A., Kolla, S.,
770 Paciolla, M.D., Sein, L.T., Buermann, W., Balasubramanian, M., Budnick, J., and Xing, B.S.
771 (1997) Tight metal binding by humic acids and its role in biomineralization. Journal of the
772 Chemical Society-Dalton Transactions(21), 4047-4060.
773 Derenne, S., and Tu, T.T.N. (2104) Characterizing the molecular structure of organic matter
774 from natural environments: An analytical challenge. Comptes Rendus Geoscience, 346 (3-4) 53-
775 63.
776 Ebrahimi, D., Whittle, A.J., and Pellenq, R. J.-M. (2014) Mesoscale properties of clay aggregates
777 from potential of mean force representation of interactions between nanoplatelets, Journal of
778 Chemical Physics, 140, 154309.
779 Ensing, B., De Vivo, M., Liu, Z., Moore, P., and Klein, M.L. (2006) Metadynamics as a tool for
780 exploring free energy landscapes of chemical reactions. Accounts of Chemical Research, 39(2),
781 73-81.
782 Ferrage, E., Sakharov, B.A., Michot, L.J., Delville, A., Bauer, A., Lanson, B., Grangeon, S.,
783 Frapper, G., Jimenez-Ruiz, M., and Cuello, G.J. (2011) Hydration properties and interlayer
784 organization of water and ions in synthetic Na-smectite with tetrahedral layer charge. Part 2.
785 Toward a precise coupling between molecular simulations and diffraction data. Journal of
786 Physical Chemistry C, 115(5), 1867-1881.
787 Fripiat, J.J., Cruz, M.I., Bohor, B.F., and Thomas, J. (1974) Interlamellar adsorption of carbon-
788 dioxide by smectites. Clays and Clay Minerals, 22(1), 23-30.
789 Fripiat, J.J., Letellier, M., and Levitz, P. (1984) Interaction of water with clay surfaces.
790 Philosophical Transactions of the Royal Society a - Mathematical Physical and Engineering
791 Sciences, 311(1517), 287-299.

Gale, J.D., (2001) Simulating the crystal structures and properties of ionic materials from interatomic potentials, Reviews in Mineralogy and Geochemistry, 42, 37-62.

Grandjean, J. (1997) Water sites at a clay interface. Journal of Colloid and Interface Science.185(2), 554-556.

Greathouse, J.A., Johnson, K.L., and Greenwell, H.C. (2014) Interaction of natural organic matter with layered minerals: recent developments in computational methods at the nanoscale. Minerals, 2014 (4) 519-540.

Greathouse, J.A., Refson, K., and Sposito, G. (2000) Molecular dynamics simulation of water mobility in magnesium-smectite hydrates. Journal of the American Chemical Society, 122(46), 11459-11464.

Hecht, A.M., Dupont, M., and Ducros, P. (1966) Etude des phenomenes de transport de l'eau adsorbee dans certains mineraux argileux par la resonance magnetique nucleaire. Bulletin de la Societe Francaise Mineralogie et de Cristallographie, 89(1), 6.

Heinz, H., Lin, T.-J., Mishra, R.K., and Emani, F.S. (2012) Thermodynamically consistent for fields for the assembly of inorganic, organic and biological nanostructures: the INTERFACE force field. Langmuir, 29, 1754-1765.

Hou, X.Q., Kalinichev, A.G., and Kirkpatrick, R.J. (2002) Interlayer structure and dynamics of Cl^--$LiAl_2$-layered double hydroxide: ^{35}Cl NMR observations and molecular dynamics modeling. Chemistry of Materials, 14(5), 2078-2085.

Hoyt, D. W., Turcu, R. V. F., Sears, J. A., Rosso, K. M., Burton, S. D., Felmy, A., and Hu, J. Z. (2011) High-pressure magic angle spinning nuclear magnetic resonance. Journal of Magnetic Resonance, 212, 378−385.

Hougardy, J., Stone, W.E.E., and Fripiat, J.J. (1977) Complex proton NMR-spectra in some ordered hydrates of vermiculites. Journal of Magnetic Resonance, 25(3), 563-567.

Iskrenova-Tchoukova, E., Kalinichev, A.G., and Kirkpatrick, R.J. (2010) Metal cation complexation with natural organic matter in aqueous solutions: Molecular dynamics simulations and potentials of mean force. Langmuir, 26(20), 15909-15919.

Kalinichev, A.G. (2001) Molecular simulations of liquid and supercritical water: Thermodynamics, structure, and hydrogen bonding. Reviews in Mineralogy and Geochemistry, 42, 83-129.

Kalinichev, A.G. (2013) Molecular models of natural organic matter and its colloidal aggregation in aqueous solutions: Challenges and opportunities for computer simulations. Pure and Applied Chemistry, 85(1), 149-158.

Kalinichev, A.G. (2014) Molecular structure and dynamics of nano-confined water: Computer simulations of aqueous species in clay, cement, and polymer membranes. In L. Mercury, N. Tas, and M. Zilberbrand, Eds. Transport and Reactivity of Solutions in Confined Hydrosystems, p. 103-115. Springer Netherlands, Dordrecht.

Kalinichev, A.G., Iskrenova-Tchoukova, E., Faraone, A., and Kirkpatrick, R.J. (2010) Molecular mechanisms of the librational motions of water in the interlayers of hydrocalumite. Geochimica et Cosmochimica Acta, 74(12), A489.

Kalinichev, A.G., Kirkpatrick, R.J., and Cygan, R.T. (2000) Molecular modeling of the structure and dynamics of the interlayer and surface species of mixed-metal layered hydroxides: Chloride and water in hydrocalumite (Friedel's salt). American Mineralogist, 85(7-8), 1046-1052.

Kalinichev, A.G., and Kirkpatrick, R.J. (2007) Molecular dynamics simulation of cationic complexation with natural organic matter. European Journal of Soil Science, 58(4), 909-917.

Kinsey, R. A., Kirkpatrick, R. J., Hower, J., Smith, K. A., and Oldfield, E. (1985) High-resolution aluminum-27 and silicon-29 nuclear magnetic resonance spectroscopic study of layer silicates, including clay minerals. American Mineralogist, 70, 537-548.

Kim, Y., Kirkpatrick, R.J., and Cygan, R.T. (1996) ^{133}Cs NMR study of cesium on the surfaces of kaolinite and illite. Geochimica et Cosmochimica Acta, 60, 4059–4074.

Kirkpatrick, R.J., Kalinichev, A.G., Wang, J., Hou, X., and Amonette, J.E. (2005a) Molecular modeling of the vibrational spectra of interlayer and surface species of layered double hydroxides. In: J.T. Kloprogge, Ed. The Application of Vibrational Spectroscopy to Clay Minerals and Layered Double Hydroxides (CMS Workshop Lecture Series v.13), p. 239-285. The Clay Minerals Society, Aurora, CO.

Kirkpatrick, R.J., Kalinichev, A.G., and Wang, J. (2005b) Molecular dynamics modelling of hydrated mineral interlayers and surfaces: structure and dynamics. Mineralogical Magazine, 69(3), 289-308.

Kirkpatrick, R.J., Kalinichev, A.G., Hou, X., and Struble, L. (2005c) Experimental and molecular dynamics modeling studies of interlayer swelling: water incorporation in kanemite and ASR gel. Materials and Structures, 38(278), 449-458.

Kirkpatrick, R.J., Yu, P., Hou, X.Q., and Kim, Y. (1999) Interlayer structure, anion dynamics, and phase transitions in mixed-metal layered hydroxides: Variable temperature ^{35}Cl NMR spectroscopy of hydrotalcite and Ca-aluminate hydrate (hydrocalumite). American Mineralogist, 84(7-8), 1186-1190.

Krishnan, M., Saharay, M., and Kirkpatrick, R.J. (2013) Molecular dynamics modeling of CO_2 and poly(ethylene glycol) in montmorillonite: The structure of clay-polymer composites and the incorporation of CO_2. Journal of Physical Chemistry C, 117(40), 20592-20609.

Kumar P.P., Kalinichev A.G., and Kirkpatrick R.J. (2006) Hydration, swelling, interlayer structure and hydrogen bonding in organo layered double hydroxides: insights from molecular dynamics simulation of citrate-intercalated hydrotalcite. Journal of Physical Chemistry B, 110, 3841-3844.

Leenheer, J.A. (2009) Systematic approaches to comprehensive analyses of natural organic matter. Annals of Environmental Science, 3, 1-130.

Li, Q, and Kirkpatrick, R.J. (2007) Organic anions in layered double hydroxides: an experimental investigation of citrate hydrotalcite. American Mineralogist, 92, 397-402.

Lippmaa, E., Mägi., M., Samosen, A., Engelhardt., G., and Grimmer, A.-R. (1980) Structural studies of silicates by solid-state high-resolution ^{29}Si NMR, Journal of the American Chemical Society, 102, 4889-4893.

Loring, J.S., Schaef, H.T., Turcu, R.V.F., Thompson, C.J., Miller, Q.R.S., Martin, P.F., Hu, J.Z., Hoyt, D.W., Qafoku, O., Ilton, E.S., Felmy, A.R., and Rosso, K.M. In situ molecular spectroscopic evidence for CO_2 intercalation into montmorillonite in supercritical carbon dioxide. Langmuir, 28(18), 7125-7128.

Marcelin, G., Stockhausen, N.J., Post, J.F.M., and Schutz, A. (1989) Dynamics and ordering of interlayered water in layered metal hydroxides. Journal of Physical Chemistry, 93, 4646 - 4650.

Marry, V., Dubois, E., Malikova, N., Durand-Vidal, S., Longeville, S., and Breu, J. (2011) Water dynamics in hectorite clays: Influence of temperature studied by coupling neutron spin echo and molecular dynamics. Environmental Science and Technology, 45(7), 2850-2855.

Marry V., Rotenberg B., and dTurq P. (2008) Structure and dynamics of water at a clay surface from molecular dynamics simulation. Physical Chemistry chemical Physics.10, 4802-4813.

Michot, L.J., Ferrage, E., Jiménez-Ruiz, M., Boehm, M., and Delville, A. (2012) Anisotropic features of water and ion dynamics in synthetic Na- and Ca-smectites with tetrahedral layer charge. A combined quasi-elastic neutron-scattering and molecular dynamics simulations study. Journal of Physical Chemistry C, 116(31), 16619-16633.

Morrow, C.P., Yazaydin, A.Ö., Krishnan, M., Bowers, G.M., Kalinichev, A.G., and Kirkpatrick, R.J. (2013) Structure, energetics, and dynamics of smectite clay interlayer hydration: Molecular dynamics and metadynamics investigation of Na-hectorite. Journal of Physical Chemistry C, 117(10), 5172-5187.

Mulla, D.J., Cushman, J.H., and Low, P.F. (1984) Molecular-dynamics and statistical-mechanics of water near an uncharged silicate surface. Water Resources Research, 20(5), 619-628.

Murphy, E. M., and Zachara, J. M. (1995) The role of sorbed humic substances on the distribution of organic and inorganic contaminants in groundwater, Geoderma , 67, 103-124.

Newman, S.P., Williams, S.J., Coveney, P.V., and Jones, W. (1998) Interlayer arrangement of hydrated MgAl layered double hydroxides containing guest terephthalate anions: Comparison of simulation and measurement. Journal of Physical Chemistry B, 102(35), 6710-6719.

Ngouana W, B.F., and Kalinichev, A.G. (2014) Structural arrangements of isomorphic substitutions in smectites: Molecular simulation of the swelling properties, interlayer structure, and dynamics of hydrated Cs-montmorillonite revisited with new clay models. Journal of Physical Chemistry C, 118(24), 12758-12773.

Piccolo, A. (2001) The supramolecular structure of humic substances, Soil Science, 166, 810-832.

Piccolo, A. (2002) The supramolecular structure of humic substances: A novel understanding of humus chemistry and implications in soil science, Advances in Agronomy, 75, 57-65.

Purcell, E., Torrey, H., and Pound, R. (1946). Resonance absorption by nuclear magnetic moments in a solid. Physical Review 69, 37-38.

Rabi, I.I., Zacharias, J.R., Millman, S., and Kusch, P. (1938). A new method of measuring nuclear magnetic moment. Physical Review 53 (4), 318–327.

Rahman, A. (1964) Correlations in motion of atoms in liquid argon. Physical Review A, 136, 405-411.

Rapin, J.P., Renaudin, G., Elkaim, E., and Francois, M. (2002) Structural transition of Friedel's salt $3CaO{\cdot}Al_2O_3{\cdot}CaCl_2{\cdot}10H_2O$ studied by synchrotron powder diffraction. Cement and Concrete Research, 32(4), 513-519.

Ritchie, J. D., and Perdue, E.M. (2003) Proton-binding study of standard and reference fulvic acids, humic acids, and natural organic matter , Geochimica et Cosmochimica Acta, 67, 85-96.

Saharay, M., and Balasubramanian, S. (2007) Evolution of intermolecular structure and dynamics in supercritical carbon dioxide with pressure: an ab initio molecular dynamics study. Journal of Physical Chemistry B, 111, 387-392.

Schaumann, G.E., and Thiele-Bruhn, S. (2011) Molecular modeling of soil organic matter: Squaring the circle? Geoderma, 166, 1-14.

Schulten, H.R., and Schnitzer, M. (1997) Chemical model structures for soil organic matter and soils. Soil Science, 162, 115–130.

Sein, L.T., Varnum, J.M., and Jansen, S.A. (1999) Conformational modeling of a new building block of humic acid: Approaches to the lowest energy conformer. Environmental Science and Technology, 33(4), 546-552.

927 Shevchenko S.M. and Bailey G.W. (1998) Non-bonded organo-mineral interactions and sorption
928 of organic compounds on soil surfaces - a model approach, Journal of Molecular Structure, 422,
929 259-270.
930 Siantar, D.P., Feinberg, B.A., and Fripiat, J.J. (1994) Interaction between organic and inorganic
931 pollutants in the clay interlayer. Clays and Clay Minerals, 42(2), 187-196.
932 Skipper, N.T., Lock, P.A., Titiloye, J.O., Swenson, J., Mirza, Z.A., Howells, W.S., and
933 Fernandez-Alonso, F. (2006) The structure and dynamics of 2-dimensional fluids in swelling
934 clays. Chemical Geology, 230(3-4), 182-196.
935 Slichter, C.P., 1990, Principles of magnetic resonance, Springer-Verlag, Berlin, 655 p.
936 Smith, D.E. (1998) Molecular computer simulations of the swelling properties and interlayer
937 structure of cesium montmorillonite. Langmuir, 14(20), 5959-5967.
938 Sposito, G. (1984) The surface chemistry of soils, Oxford University Press, New York, 234 p.
939 Stefánsson, A., Driesner, T., and Benezeth, P., Eds. (2013) Thermodynamics of geothermal
940 fluids, 350 p., Reviews in Mineralogy and Geochemistry, 76 .
941 Stevenson, F.J. (1994) Humus Chemistry: Genesis, Composition, Reactions. John Wiley, New
942 York.
943 Sullivan, D.J., Shore, J.S., and Rice, J.A. (2000) ^{113}Cd double-resonance NMR as a probe of clay
944 mineral cation exchange sites. American Mineralogist, 85(7-8), 1022-1029.
945 Sutton, R., and Sposito, G. (2005) Molecular structure in soil humic substances: The new view.
946 Environmental Science and Technology, 39(23), 9009-9015.
947 Sutton, R., and Sposito, G. (2006) Molecular simulation of humic substance - Ca-
948 montmorillonite complexes. Geochimica et Cosmochimica Acta, 70(14), 3566-3581.

949 Sutton, R., Sposito, G., Diallo, M.S., and Schulten, H.R. (2005) Molecular simulation of a model
950 of dissolved organic matter. Environmental Toxicology and Chemistry, 24(8), 1902-1911.
951 Suzuki, M., and Schnepp, O. (1971) Intermolecular potential and lattice dynamics of the CO_2
952 crystal. Journal of Chemical Physics, 55, 5349-5356.
953 Teich-McGoldrick, S.L., Greathouse, J.A., and Cygan, R.T., (2014) Molecular dynamics
954 simulations of uranyl adsorption and structure on the basal surface of muscovite, Molecular
955 Simulation, 40 (7-9) 610-617.
956 Teppen, B.J., Rasmussen, K., Bertsch, P.M., Miller, D.M., and Schafer, L. (1997) Molecular
957 dynamics modeling of clay minerals. 1. Gibbsite, kaolinite, pyrophyllite, and beidellite. Journal
958 of Physical Chemistry B, 101(9), 1579-1587.
959 Terzis, A., Filippakis, S., Kuzel, H.J., and Burzlaff, H. (1987) The crystal structure of
960 $Ca_2Al(OH)_6Cl{\cdot}2H_2O$. Zeitschrift fur Kristallographie, 181(1-4), 29-34.
961 Tipping, E. (2002) Cation binding by humic substances. 434 p. Cambridge University Press,
962 Cambridge.
963 Touillaux R, Salvador, P., Vandermeersche C, and Fripiat, J.J. (1968) Study of water layers
964 adsorbed on Na- and Ca-montmorillonite by pulsed nuclear magnetic resonance technique. Israel
965 Journal of Chemistry, 6(3), 337-348.
966 Vega, C., Sanz, E., and Abascal, J.L.F. (2005) The melting temperature of the most common
967 models of water. Journal of Chemical Physics, 122(11), 114507-1-9.
968 Wang, J.W., Kalinichev, A.G., Kirkpatrick, R.J., and Hou, X.Q. (2001) Molecular modeling of
969 the structure and energetics of hydrotalcite hydration. Chemistry of Materials, 13(1), 145-150.

970 Wang, J.W., Kalinichev, A.G., Kirkpatrick, R.J., and Cygan, R.T. (2005) Structure, energetics,
971 and dynamics of water adsorbed on the muscovite (001) surface: A molecular dynamics
972 simulation. Journal of Physical Chemistry B, 109(33), 15893-15905.
973 Wang, J.W., Kalinichev, A.G., and Kirkpatrick, R.J. (2006) Effects of substrate structure and
974 composition on the structure, dynamics, and energetics of water at mineral surfaces: A molecular
975 dynamics modeling study. Geochimica et Cosmochimica Acta, 70(3), 562-582.
976 Wang, Y., Wohlert, J., Berglund, L.A., Tu, Y.Q., and Agren, H. (2014) Molecular dynamics
977 simulation of strong interaction mechanisms at wet interfaces in clay-polysaccharide
978 nanocomposites, Journal of Materials Chemistry, 2 (25), 9541-9547.
979 Weiss, C. A., Jr., Altaner, S. P., and Kirkpatrick, R. J. (1987) High-resolution ^{29}Si NMR
980 spectroscopy of layer silicates: correlations between chemical shift and structural distortions.
981 American Mineralogist, 72, 935-942.
982 Weiss, C.A., Kirkpatrick, R.J., and Altaner, S.P. (1990) The structural environments of cations
983 adsorbed onto clays - ^{133}Cs variable-temperature MAS NMR spectroscopic study of hectorite.
984 Geochimica et Cosmochimica Acta, 54(6), 1655-1669.
985 Wershaw, R.L. (2004) Evaluation of conceptual models of natural organic matter (humus) from a
986 consideration of the chemical and biochemical processes of humification. U.S. Geological
987 Survey Scientific Investigations Report 2004-5121, Reston, VA.
988 Wershaw, R.L., Thorn, K.A., and Pinckney, D.J., (1988) Characterization of humic-acid
989 fractions by C-13 nuclear magnetic resonance spectroscopy, Environmental Technology Letters,
990 9(1) 53-62.
991 Wittebort, R. J.; Usha, M.G.; Ruben, D.J.; Wemmer, D.E.; Pines, A. (1998) Observation of

molecular reorientation in ice by proton and deuterium magnetic resonance, Journal of the American Chemical Society, 110, 5668-5671.

Woessner, D.E., and Snowden, B.S. (1969) A study of orientation of adsorbed water molecules on montmorillonite clays by pulsed NMR. Journal of Colloid and Interface Science, 30(1), 54-68.

Xu, X., Kalinichev, A.G., and Kirkpatrick, R.J. (2006) ^{133}Cs and ^{35}Cl NMR spectroscopy and molecular dynamics modeling of Cs^+ and Cl^- complexation with natural organic matter. Geochimica et Cosmochimica Acta, 70(17), 4319-4331.

Figure captions

Figure 1. ^{133}Cs MAS NMR spectra of Cs-exchanged hectorite in a 1.0M CsCl slurry collected at 20^o and -100^{o}C . See text for explanation. After Weiss et al. (1990).

Figure 2. ^{23}Na MAS NMR spectra of Na-exchanged hectorite collected at an H_0 field of 9.4T and the indicated temperatures. Spectra for samples equilibrated at 43% relative humidity (labeled "low H_2O") and over P_2O_5 are shown for comparison. See text for discussion. After Bowers et al. (2011).

Figure 3. ^{2}H static NMR spectra of Na-exchanged hectorite collected at an H_0 field of 7.0T and the indicated temperatures. The left panel shows spectra for a 1.5:1 paste and the right panel spectra for a sample equilibrated at 43% relative humidity (termed "low H_2O"). See text for discussion. After Bowers et al. (2011).

Figure 4. ^{2}H NMR spectra calculated assuming different models of restricted water molecule dynamical motions in the fast motion limit between -50°C and -20°C compared to experimental spectra obtained at -50°C for (a) Na-hectorite with dominantly 2 water layers, (b) Na-hectorite paste, and (c) K-hectorite paste. Models include (d) the fast limit C_2/C_3 model rotational model

discussed in the text, (e) jump motion about a C_2 director alone, and (f) tetrahedral jump motion. No line-broadening was added to the model spectra.

Figure 5. Definition of angles used in smectite interlayer water dynamics. θ is the angle between the normal to the clay layer and vector between a cation and an O_{H2O}. ω is the angle between the normal to the clay layer and the bisector for the H-O-H angle of a water molecules (the dipole direction). φ is the angle between two O_{H2O} and a cation.

Figure 6. ^{133}Cs NMR $1/T_1$ relaxation rates of CsCl-Suwannee NOM solutions and neat CsCl solutions collected at room temperature and the indicated pH values. The $1/T_1$ relaxation rates increase with Cs/NOM ratio and pH, whereas the values for the neat solutions do not change significantly with pH, demonstrating increasing Cs-NOM interaction with increasing pH. After Yu et al. (2006).

Figure 7. ^{23}Na MAS NMR spectra of a) Na-exchanged hectorite and b) a Na-hectorite-Suwannee River humic acid composite collected at 50°C. For both samples the red spectrum was collected at P_{CO2} = 90 bars and the black spectrum at atmospheric pressure. See text for discussion. After Bowers et al. (2014).

Figure 8: Computed probability density isosurfaces of oxygen atoms around CO_2 that belong to the first coordination shell of interlayer CO_2 molecules in MD simulations of a montmorillonite-CO_2-(poly)ethylene glycol system. (a) O_{CO2}, (b) O_{PEG}. Blue: $r(C_{CO2} – O) < 3.34$Å. Magenta: $3.34Å < r(C_{CO2} – O) < 5.7$Å. Red: O of the central CO_2 molecule. The C_{CO2} is hidden behind the blue isosurface. This coordination is very similar to that in supercritical CO_2 (Saharay and Balasubramanian, 2007) and also to the dry ice structure. After Krishnan, et al. (2013).

Figure 9. Static ^{35}Cl NMR spectra of hydrocalumite collected at the indicated temperatures. H_0 = 11.7T. The change in peak shape between 0 and 10^{o}C reflects a structural phase transition. See text for discussion. After Kirkpatrick et al. (1999).

Figure 10. ^{35}Cl static and MAS NMR spectra of a Li-Al layered double hydroxides collected under the conditions indicated. H_0 = 11.7 T. The inset in spectrum j is the same spectrum as the main one in j, but the horizontal scale is much expanded to highlight the quadrupolar contribution to the line shape. See text for discussion. After Hou et al. (2002).

Figure 11. Representative structural environments of Cl^- and H_2O in the interlayer of Li-Al layered double hydroxide (a) Cl^- ion located in a distorted octahedral environment showing H-bond donation to it from H_2O and -OH viewed from a direction parallel to the layers with an interlayer content of 1 Cl^- and 1 H_2O per formula unit. (b) same structure as in (a) but viewed perpendicular to the interlayer. (c) Cl^- ion in a trigonal prismatic environment of OH groups for the fully dehydrated phase. Green balls = Cl-, red balls = O of water or OH, white balls = H of water or OH, pink octahedron = Al of hydroxide layer, and blue balls = Li of hydroxide layer. (shown not to scale to improve visibility in figures a and b**)**. See text for discussion. After Hou et al. (2002).

1053

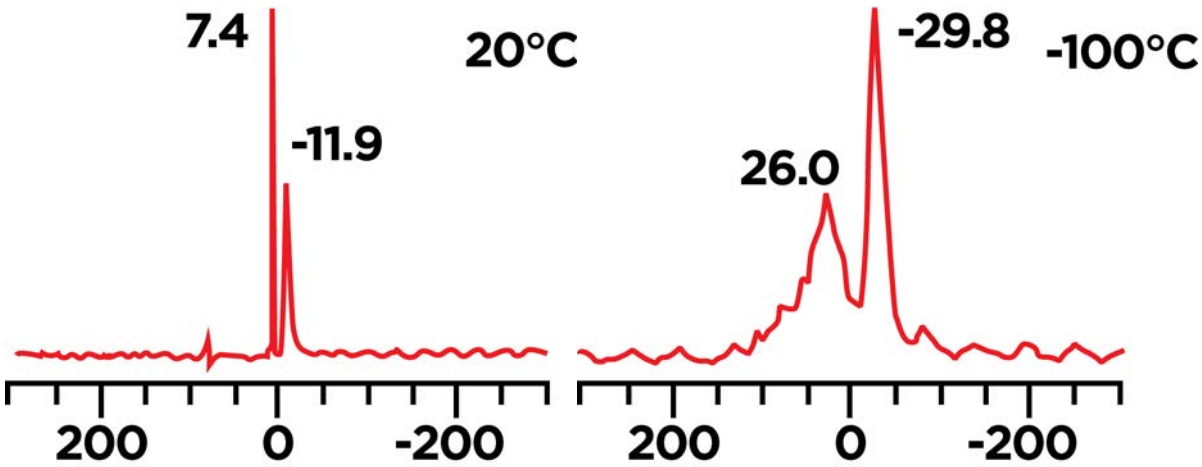

1054

1055 Figure 1. ^{133}Cs MAS NMR spectra of Cs-exchanged hectorite in a 1.0M CsCl slurry collected at

1056 20^{o} and -100^{o}C . See text for explanation. After Weiss et al. (1990).

1057

1058

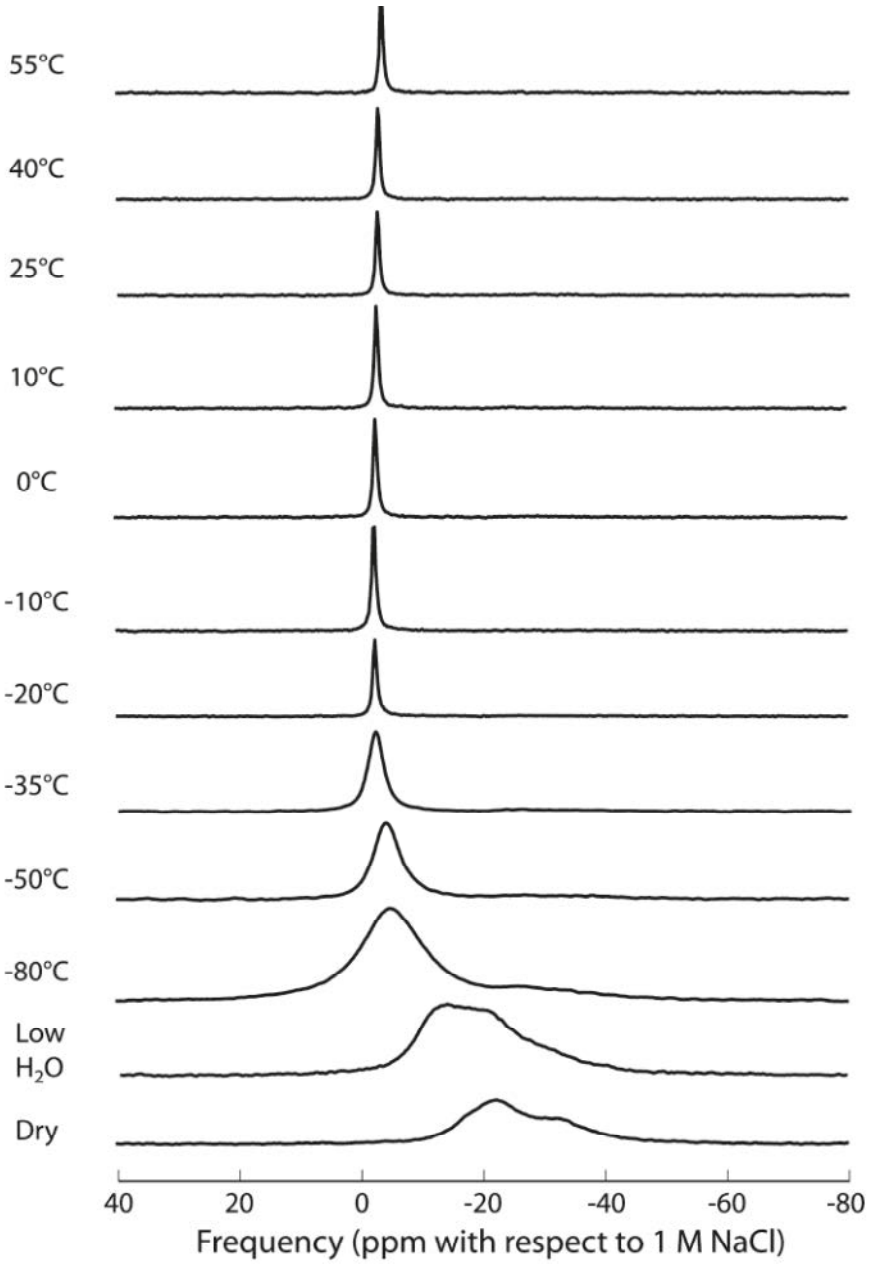

1059

1060 Figure 2. ^{23}Na MAS NMR spectra of Na-exchanged hectorite collected at an H_0 field of 9.4T and
1061 the indicated temperatures. Spectra for samples equilibrated at 43% relative humidity (labeled
1062 "low H_2O") and over P_2O_5 are shown for comparison. See text for discussion. After Bowers et
1063 al. (2011).

1064

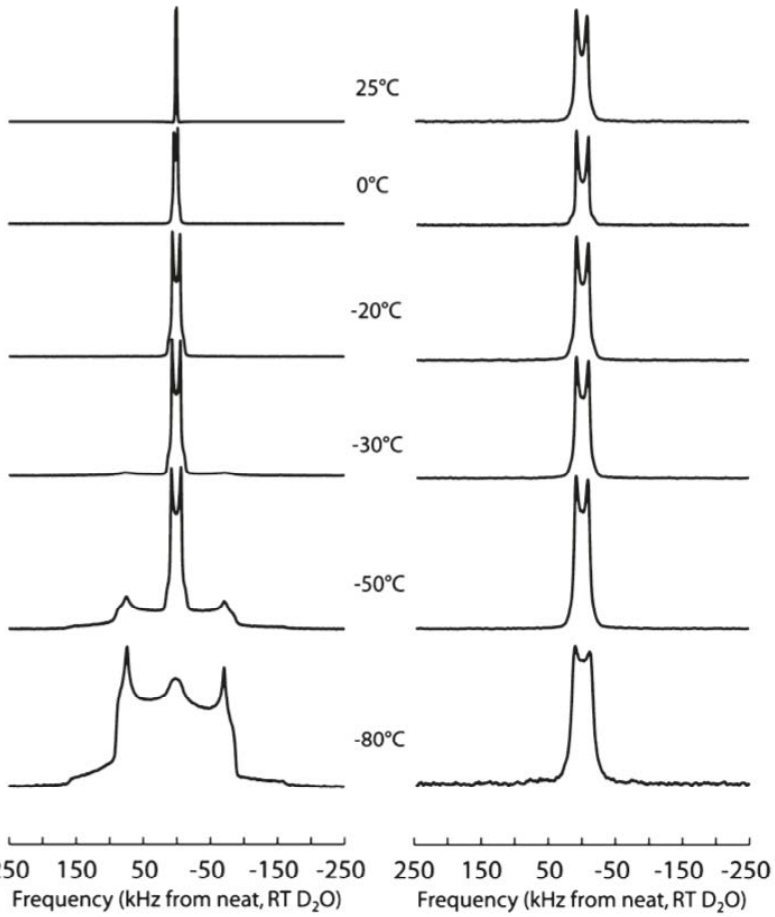

Figure 3. ^{2}H static NMR spectra of Na-exchanged hectorite collected at an H_0 field of 7.0T and the indicated temperatures. The left panel shows spectra for a 1.5:1 paste and the right panel spectra for a sample equilibrated at 43% relative humidity (termed "low H_2O"). See text for discussion. After Bowers et al. (2011).

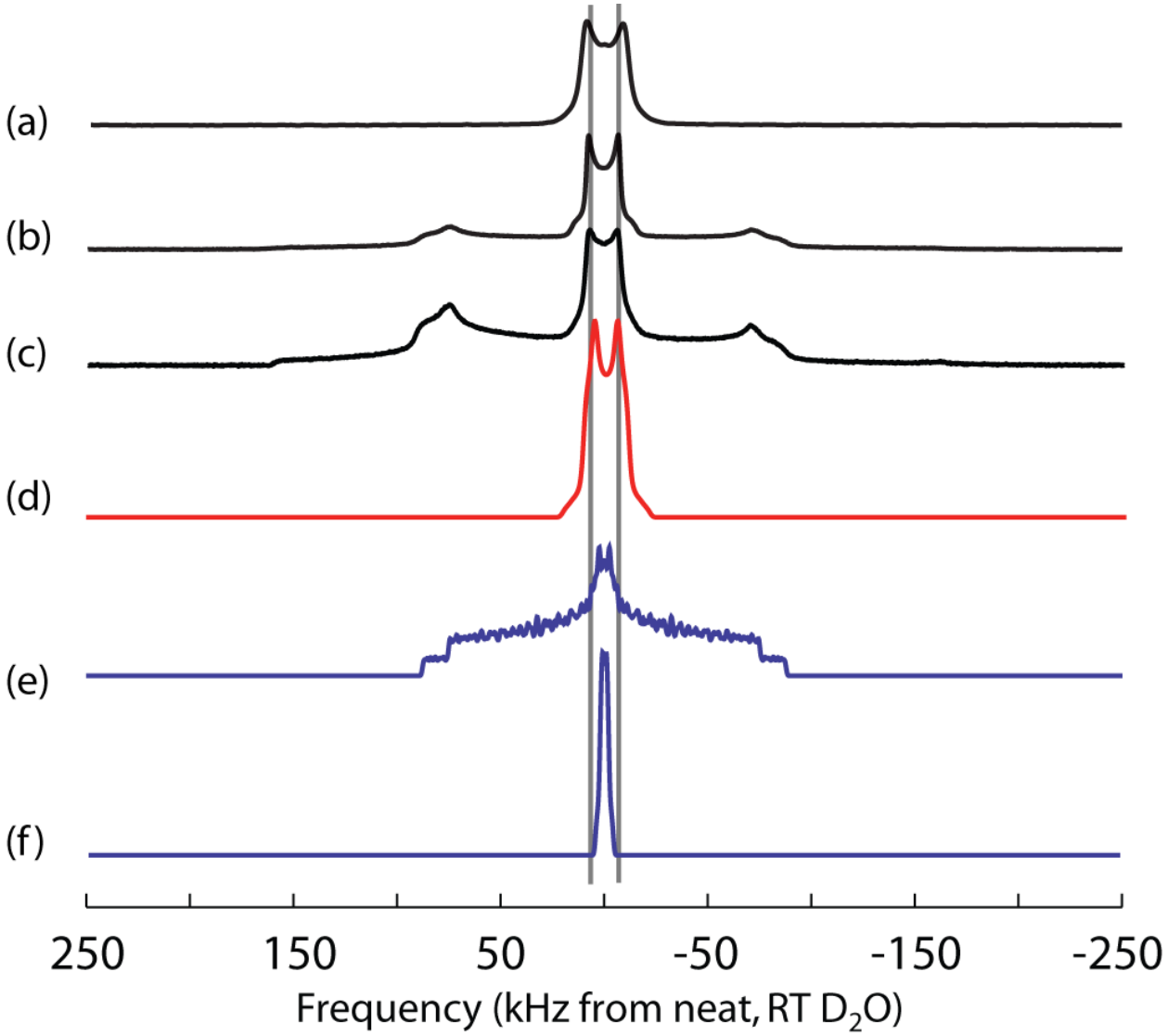

Figure 4. ^{2}H NMR spectra calculated assuming different models of restricted water molecule dynamical motions in the fast motion limit between -50°C and -20°C compared to experimental spectra obtained at -50°C for (a) Na-hectorite with dominantly 2 water layers, (b) Na-hectorite paste, and (c) K-hectorite paste. Models include (d) the fast limit C_2/C_3 model rotational model discussed in the text, (e) jump motion about a C_2 director alone, and (f) tetrahedral jump motion. No line-broadening was added to the model spectra.

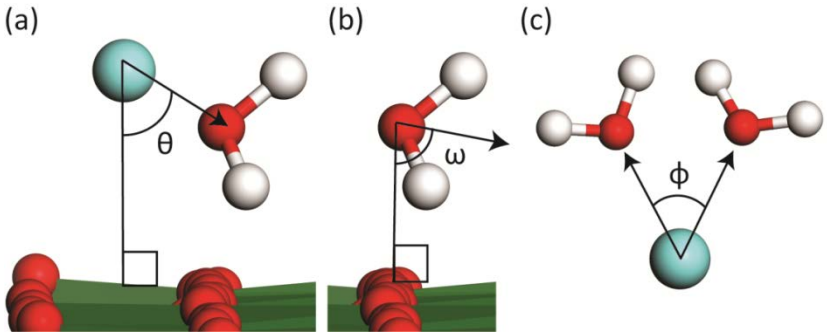

Figure 5. Definition of angles used in smectite interlayer water dynamics. θ is the angle between the normal to the clay layer and vector between a cation and an O_{H2O}. ω is the angle between the normal to the clay layer and the bisector for the H-O-H angle of a water molecules (the dipole direction). φ is the angle between two O_{H2O} and a cation.

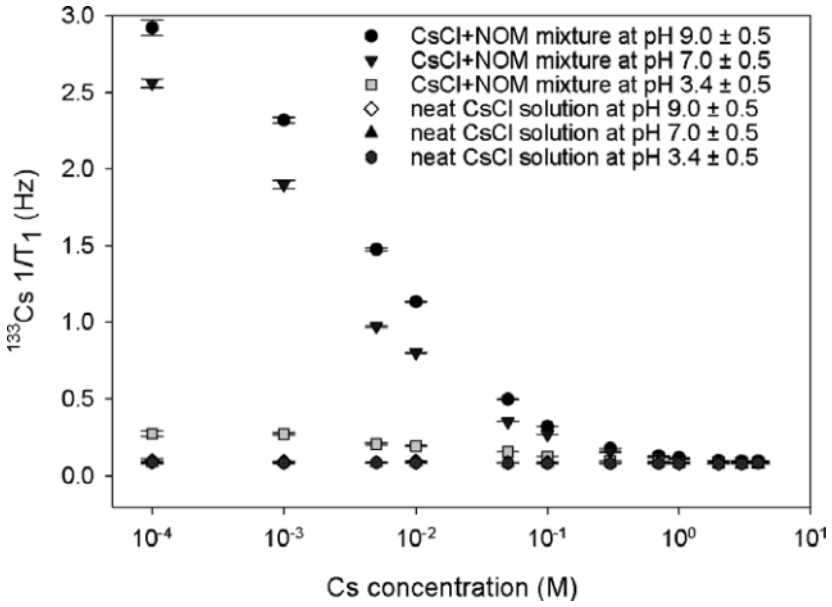

Figure 6. ^{133}Cs NMR $1/T_1$ relaxation rates of CsCl-Suwannee NOM solutions and neat CsCl solutions collected at room temperature and the indicated pH values. The $1/T_1$ relaxation rates increase with Cs/NOM ratio and pH, whereas the values for the neat solutions do not change significantly with pH, demonstrating increasing Cs-NOM interaction with increasing pH. After Yu et al., 2006.

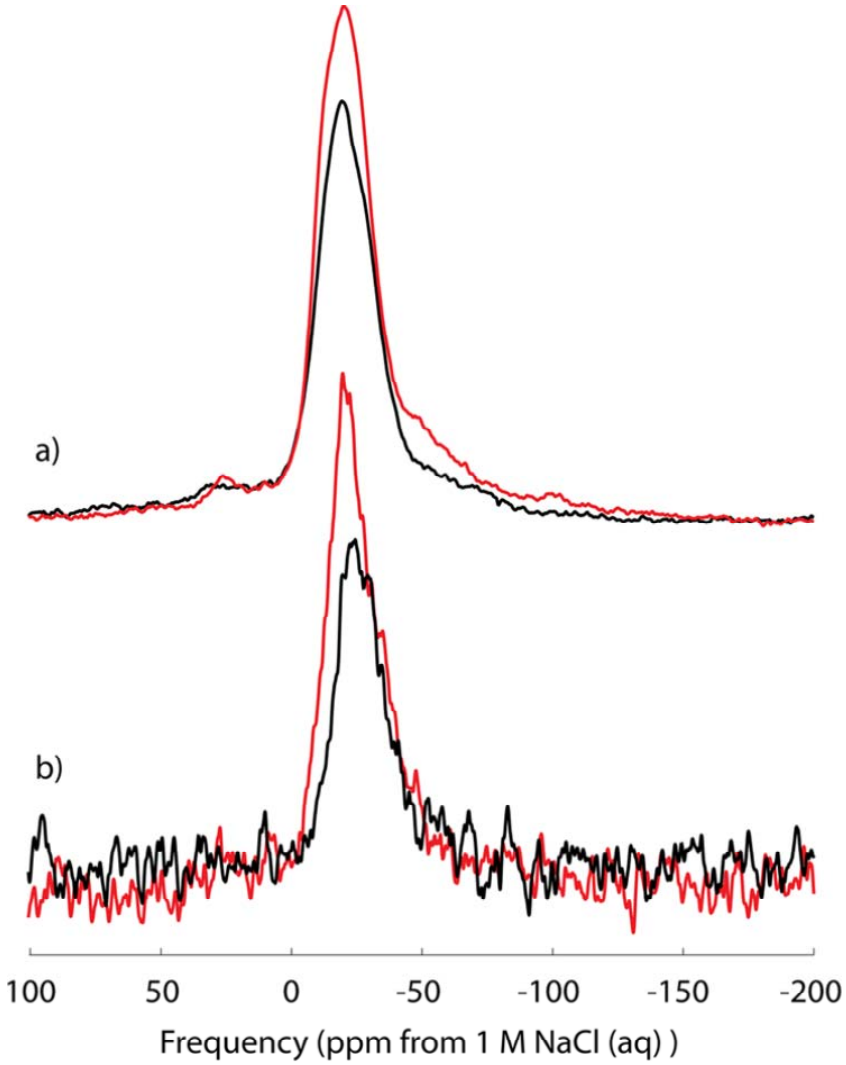

Figure 7. ^{23}Na MAS NMR spectra of a) Na-exchanged hectorite and b) a Na-hectorite-Suwannee River humic acid composite collected at 50°C . For both samples the red spectrum was collected at P_{CO2} = 90 bars and the black spectrum at atmospheric pressure. See text for discussion. After Bowers et al., 2014.

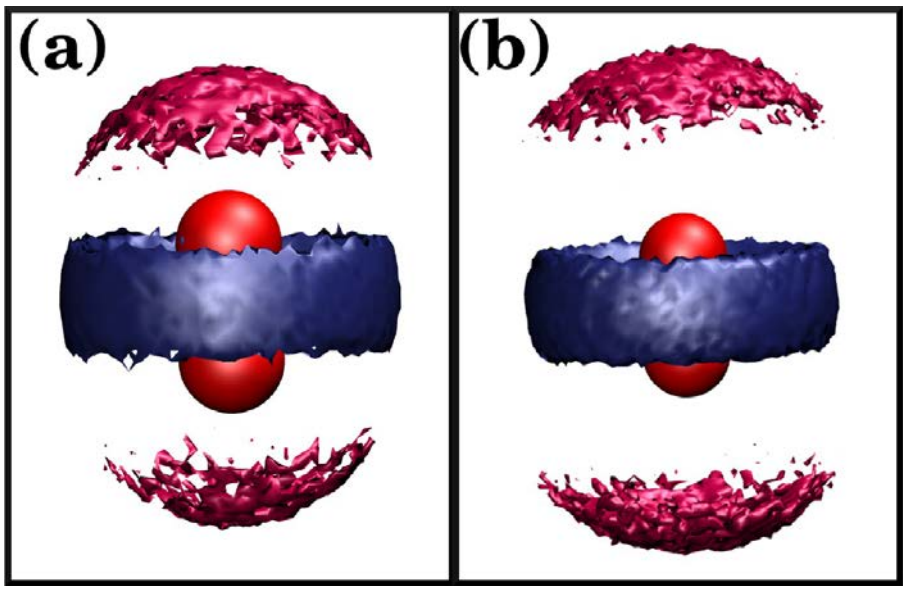

Figure 8: Computed probability density isosurfaces of oxygen atoms around CO_2 that belong to the first coordination shell of interlayer CO_2 molecules in MD simulations of a montmorillonite-CO_2-(poly)ethylene glycol system. (a) O_{CO2}, (b) O_{PEG}. Blue: $r(C_{CO2} – O) < 3.34$Å. Magenta: 3.34Å$< r(C_{CO2} – O) < 5.7$Å. Red: O of the central CO_2 molecule. The C_{CO2} is hidden behind the blue isosurface. This coordination is very similar to that in supercritical CO_2 (Saharay and Balasubramanian, 2007) and also to the dry ice structure. After Krishnan, et al., 2013.

1136

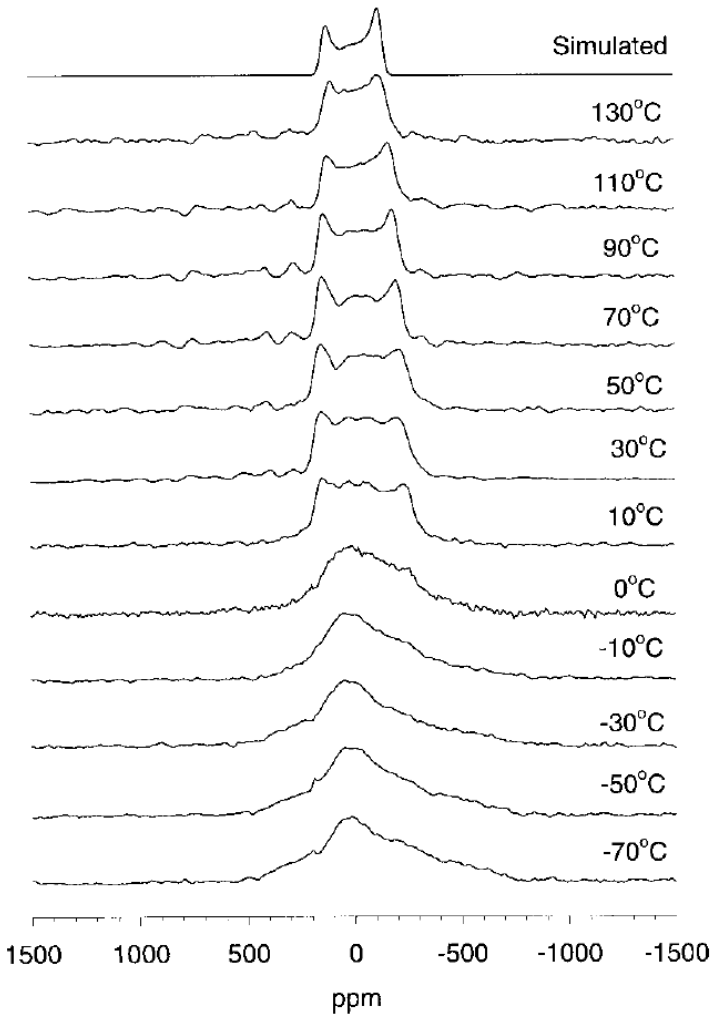

1137

1138 Figure 9. Static ^{35}Cl NMR spectra of hydrocalumite collected at the indicated temperatures. H_0 =

1139 11.7T. The change in peak shape between 0 and 10°C reflects a structural phase transition. See

1140 text for discussion. After Kirkpatrick et al., 1999.

1141

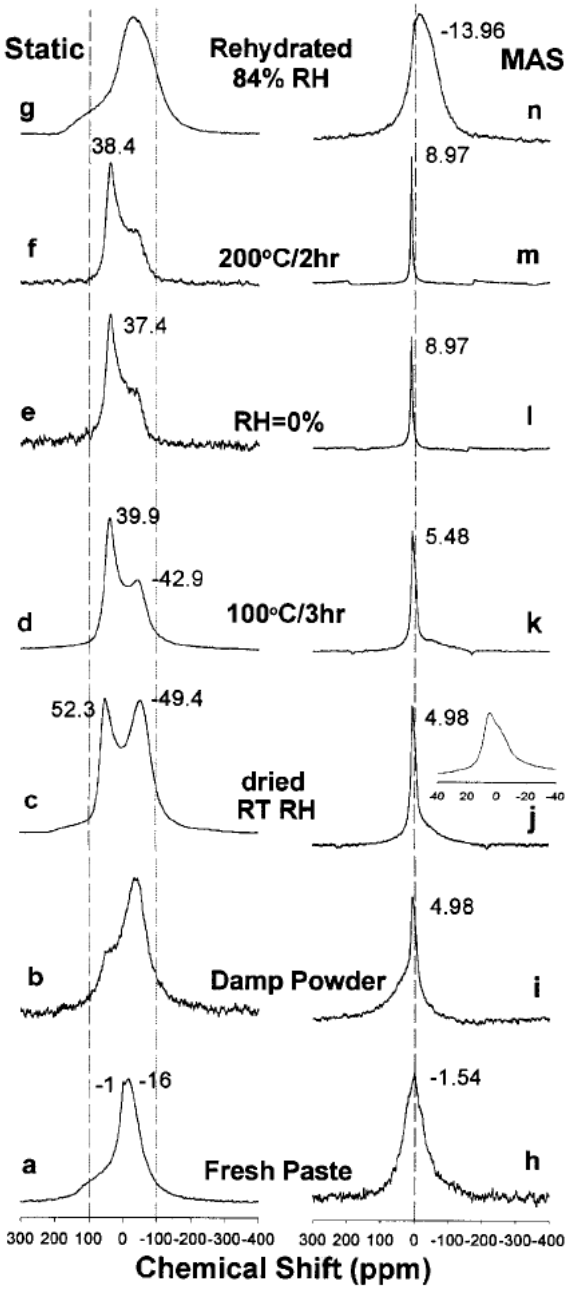

Figure 10. ^{35}Cl static and MAS NMR spectra of a Li-Al layered double hydroxides collected under the conditions indicated. H_0 = 11.7 T. The inset in spectrum j is the same spectrum as the main one in j, but the horizontal scale is much expanded to highlight the quadrupolar contribution to the line shape. See text for discussion. After Hou et al., 2002.

1148

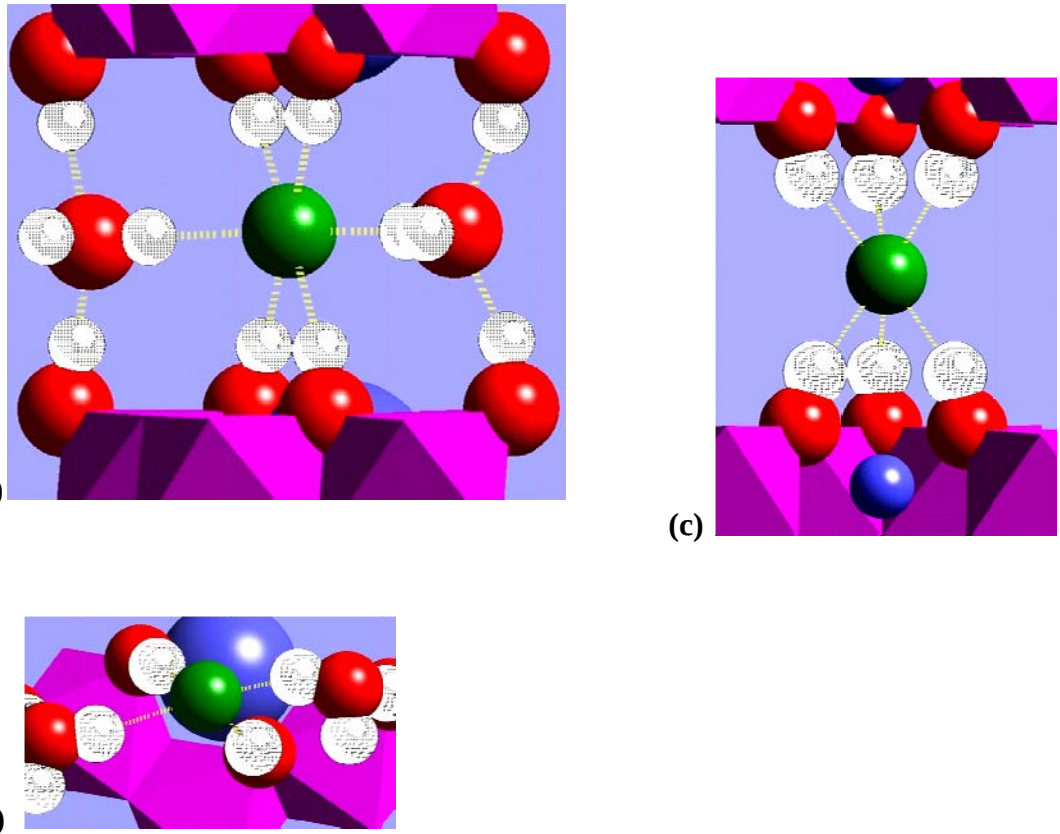

1149

1150

1151 Figure 11. Representative structural environments of Cl^- and H_2O in the interlayer of Li-Al
1152 layered double hydroxide (a) Cl^- ion located in a distorted octahedral environment showing H-
1153 bond donation to it from H_2O and -OH viewed from a direction parallel to the layers with an
1154 interlayer content of 1 Cl^- and 1 H_2O per formula unit. (b) same structure as in (a) but viewed
1155 perpendicular to the interlayer. (c) Cl^- ion in a trigonal prizmatic environment of OH groups for
1156 the fully dehydrated phase. Green balls = Cl-, red balls = O of water or OH, white balls = H of
1157 water or OH, pink octahedron = Al of hydroxide layer, and blue balls = Li of hydroxide layer.
1158 (shown not to scale to improve visibility in figures a and b**)**. See text for discussion. After Hou et
1159 al., 2002.